Preserving Linear Design Capabilities in the Nonlinear Control of Nonholonomic Autonomous Underwater Vehicles

Aristide Santos, Robert Bitmead

INRIA

INSTITUT NATIONAL DE RECHERCHE EN INFORMATIQUE ET EN AUTOMATIQUE

Preserving Linear Design Capabilities in the Nonlinear Control of Nonholonomic Autonomous Underwater Vehicles

Aristide Santos, Robert Bitmead

N° 2606

Juillet 1995

PROGRAMME 4

ISSN 0249-6399

INRIA
SOPHIA ANTIPOLIS

Preserving Linear Design Capabilities in the Nonlinear Control of Nonholonomic Autonomous Underwater Vehicles

Aristide Santos*, Robert Bitmead**

Programme 4 — Robotique, image et vision
Projet ICARE

Rapport de recherche n°2606 — Juillet 1995 — 61 pages

Abstract: We derive here an approach to the nonlinear control of a particular autonomous underwater vehicle architecture. This approach is based on state-variable feedback and estimation in the nonlinear setting but uses many techniques from Linear Quadratic Gaussian methods which are capable of preserving the design aspects of the formulation. The specific task that we consider is the tracking of an unknown ocean floor using current altitude measurements. By guarding the linear aspects as long as possible, we are able to formulate this problem as one of classical disturbance rejection in which *a priori* information about the ocean floor may be easily included. The migration from linear to nonlinear control is then performed so as to preserve as many linear design features as is possible.

Key-words: autonomous underwater vehicles (AUV), *a priori* unknown environment, AUV–environment interaction, LQ control, Kalman filtering, nonlinear estimation, nonlinear control.

(Résumé : tsvp)

This work is supported by Ifremer and by the PACA Region (FRANCE), is part of the EEC MAST II program under grant CT92-0028, and was initiated during a stay of Pr R. Bitmead as an invited professor at INRIA supported by the French Ministry for Higher Education and Research. The second author acknowledges the support of the Cooperative Research Centre for Robust & Adaptive Systems and of Australian Commonwealth Government through its funding of the Cooperative Research Centres Program.

*E-mail : santos@sophia.inria.fr
**Cooperative Research Centre for Robust & Adaptive Systems, Dept Systems Engineering, Australian National University, Canberra ACT 0200 AUSTRALIA. E-mail : bob@alfred.anu.edu.au

Unité de recherche INRIA Sophia-Antipolis
2004 route des Lucioles, BP 93, 06902 SOPHIA-ANTIPOLIS Cedex (France)
Téléphone : (33) 93 65 77 77 — Télécopie : (33) 93 65 77 65

De la Commande Linéaire à la Commande Non-Linéaire des Véhicules Sous-Marins Autonomes Non-Holonomes

Résumé : Nous développons une approche vers la commande non-linéaire d'une architecture particulière de véhicules autonomes sous-marins. Cette approche est basée sur le retour d'état et l'estimation non-linéaires, mais utilise certains résultats dérivés des méthodes Linéaires Quadratriques Gaussiennes. Le problème auquel nous nous consacrons est le suivi d'un fond de mer *a priori* inconnu par utilisation des données sensorielles issues de capteurs acoustiques. En préservant le plus longtemps possible les caractéristiques linéaires du problème, nous sommes en mesure de reformuler le problème sous la forme classique de la réjection de perturbation, dans laquelle des informations a priori sur le fond peuvent être aisément incluses. La migration de la comnande linéaire vers la commande non-linéaire est alors effectuée de manière à conserver le plus de caractéristiques linéaires possibles.

Mots-clé : véhicules autonomes sous-marins (AUVs), environnement *a priori* inconnu, intéraction AUV–environnement, commande LQ, filtrage de Kalman, estimation non-linéaire, commande non-linéaire.

1 Introduction

We consider the design of a feedback controller for an autonomous underwater vehicle (AUV) the task of which is to follow the ocean floor at a prescribed distance while generating a detailed sonar map of the floor beneath it [Masson et al., 1994]. The AUV is controlled by steerable wings at the rear and by a variable speed propeller. The current altitude is given through altitude sensors. The feedback is from this altitude sensor information to the AUV inputs, notably the wings turning. This system is nonlinear with certain features of nonminimum-phase and nonholonomic behaviour. The distance of the AUV from the ocean floor describes the interaction of the machine with its environment. The ocean floor is assumed *a priori* unknown, although statistical and rate-of-change features may be known or assumed beforehand. Our aim in this paper will be to explore the design aspects of the controller for this nonlinear AUV problem while trying to preserve as much as possible insights and formulations from linear control design. Some approaches dealing with different types of actuated AUVs have already been developed. Regarding holonomic vehicles, Task-Function approach has been applied [Santos et al., 1994a, Santos et al., 1994b, Santos et al., 1995a], while Lyapunov-based nonlinear control design has proven efficiency for plan canard actuated vehicles [Santos et al., 1995b]. However these approaches cannot be generalized to the class of rear-actuated vehicles.

The class of nonlinear systems is sometimes referred to as *the class of not-necessarily-linear systems*, which indicates the enormous range of possible members. Control design methodologies for this class inherently find difficulties in providing general approaches. Feedback linearization [Isidori, 1989], backstepping [Krstic et al., 1995], passivity [Slotine and Li, 1991] approaches rely upon specific structure of the state-variable equations describing the target system, with some of these effectively requiring invertibility. With nonholonomic mechanical systems, where certain acceleration directions are prohibited, this can lead to control feasibility problems. Similarly when constraints are added, both feasibility and design aspects may be lost. Issues of robustness and tuning of the controller to its application also are hard to address. One recent very promising approach has been the development of nonlinear predictive control methods by [Mayne and Michalska, 1990, Michalska and Mayne, 1993], which use a local model of the plant behaviour as the basis for a constrained, finite-horizon optimal control calculation. Some robustness theory has also been provided for these approaches [Michalska and Mayne, 1993], although the currently available techniques rely on full state measurement.

The tack which we pursue is to develop further this connection to predictive control, since these methods have found considerable acceptance with practitioners, particularly in the chemical process industries where models are barely adequate at best and where the central problems of disturbance rejection

need to be conducted in an uncertain environment,[Morari and Zafiriou, 1989]. A central thesis of the book [Bitmead et al., 1990] is that, in the absence of constraints and nonlinear models, many predictive control approaches (and Generalized Predictive Control of [Clarke et al., 1987, Clarke and Mohtadi, 1989] in particular) become identical to receding-horizon Linear Quadratic Gaussian (LQG) control, with the output predictions deriving from a Kalman filter. Accordingly, we explore the application of LQG-based design procedures to the AUV control problem with the eventual desire to develop a more complete observer-based nonlinear predictive controller.

The structure of the paper is as follows. In Section 2 we present the mathematical model of the AUV dynamics. Section 3 is devoted to the development of a linearized control problem formulation, which we use as the basis for design. Section 4 describes the features of the control design, the performance of which is illustrated in Section 5. Section 6 investigates the nonlinear design from the EKF extension to the fully nonlinear controller design. Section 7 concludes. Our aims are manifold :

- to develop the control design for the AUV,
- to explore the possibilities for carrying over linear design methods into a nonlinear context,
- to investigate an approach to observer-based nonlinear predictive design.

2 Description of the vehicle

The AUV is illustrated in Figure 1 in relation to the ocean floor. It is based on a vessel funded by the European Union MAST II Program to be used to create accurate surveys of the ocean floor, storing data from a carried load sensor. It is actuated through one axial screw propeller and a pair of rear symmetric wings. One of its envisaged principal mode of operation will be to follow a pre-specified straight line in absolute coordinates while remaining a constant distance y_0 above the ocean floor and moving at a strictly positive nominal axial advancement velocity u_0. Local measurements only of the altitude of the floor from the AUV are assumed to be available and feedback will be used to control this altitude via the *symmetric* wings turning.

We consider the motion of the AUV in only the (OXZ)-plane, as such a vehicle has a vertical symmetric plane leading to no coupling effect with the horizontal plane from an initiated vertical motion. We then define the following AUV variables, which are depicted in Figure 1 :

u (*surge*), the forward velocity of the AUV in its local frame (Cxyz) along its (Cx)-axis; it is always strictly positive in our case,

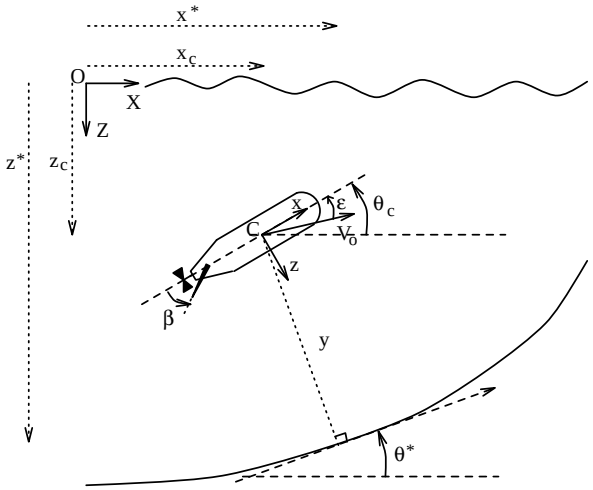

Figure 1: Autonomous underwater vehicle for bottom tracking and its environment — notations

- w (*heave*), the vertical velocity of the AUV along its (Cz)-axis,
- q (*pitch*), the angular velocity of the AUV around its (Cy)-axis,
- x_c the x-coordinate of the origin point of the AUV local frame, C, in the absolute frame of reference $(OXYZ)$,
- z_c the z-coordinate of C in the absolute frame of reference; it is measured positive in a downwards sense,
- θ_c (*trim* or *pitch angle*), the angular orientation of the AUV relative to the absolute frame of reference $(OXYZ)$,
- β the AUV wings turning relative to its (Cx)-axis measured in the vertical plane,
- ν the propeller rotation frequency.

These first six quantities will form the state-variables of the AUV, while β and ν define the process inputs.

Newtonian mechanics provides us with a simple formulation of the state dynamics :

$$\begin{aligned}\mathbf{M}_I \begin{pmatrix} \dot{u}(t) \\ \dot{w}(t) \\ \dot{q}(t) \end{pmatrix} &= m\,q(t) \begin{pmatrix} 0 & 1 & 0 \\ -1 & 0 & 0 \\ 0 & 0 & 0 \end{pmatrix} \begin{pmatrix} u(t) \\ w(t) \\ q(t) \end{pmatrix} + u(t)\,\mathbf{D}_h \begin{pmatrix} u(t) \\ w(t) \\ q(t) \end{pmatrix} \\ &\quad + \mathbf{\Gamma}_g(t) + \mathbf{U}_{cw}(t) + \mathbf{U}_{cp}(t) \qquad (1) \\ \begin{pmatrix} \dot{x}_c(t) \\ \dot{z}_c(t) \\ \dot{\theta}_c(t) \end{pmatrix} &= \begin{pmatrix} \cos(\theta_c(t)) & \sin(\theta_c(t)) & 0 \\ -\sin(\theta_c(t)) & \cos(\theta_c(t)) & 0 \\ 0 & 0 & 1 \end{pmatrix} \begin{pmatrix} u(t) \\ w(t) \\ q(t) \end{pmatrix}, \qquad (2)\end{aligned}$$

where,

$\mathbf{M}_I$ is the inertia matrix of the AUV depending on its mass m, its moment of inertia I_{yy}, the vehicle geometry, and the corrections for added water mass and inertia.

$\mathbf{D}_h$ is the negative definite (but not necessarily symmetric) matrix of drag coefficients, which satisfies a dissipation inequality,

$\mathbf{\Gamma}_g$ is the gravitation and buoyancy term.

$\mathbf{U}_{cw}$ is the force and moment introduced by the wings turning, and

$\mathbf{U}_{cp}$ is the force and moment introduced by the propeller rotation.

Note : It is worth noting that external perturbations effects such as water currents are not taken into account in this study, although they are easily included into the formulation.

To refine further the control forces, we need to introduce two more derived variables : ε the angle of incidence (see Figure 1) measured between the AUV local Cx-axis and its velocity vector $\mathbf{V}$ in the vertical plane, and J_p the propeller advancement coefficient, that are defined below :

$$V^2 \triangleq u^2 + w^2 \tag{3}$$

$$\varepsilon \triangleq \sin^{-1}(\frac{w}{V}) \triangleq \cos^{-1}(\frac{u}{V}) \tag{4}$$

$$J_p \triangleq \frac{u}{|\nu D_p|} \tag{5}$$

where D_p is the screw propeller diameter.

Then we have a convenient but representative model :

$$C_{xsw} \triangleq -(C_{xow} + c_w \frac{(C_{zow}(\varepsilon+\beta))^2}{2\pi\ b_w})$$

$$C_{zsw} \triangleq -(C_{zow}\ (\varepsilon+\beta) + 2.1\ (\varepsilon+\beta)^2)$$

$$\mathbf{U}_{cw} = \begin{pmatrix} 0.5\rho S_w V^2(C_{zsw}\sin(\beta) + C_{xsw}\cos(\beta)) \\ 0.5\rho S_w V^2(C_{zsw}\cos(\beta) - C_{xsw}\sin(\beta)) \\ 0.5\rho S_w V^2\left[-U_{cw}(2)(-0.2c_w\cos(\beta) + d_{aw}) + U_{cw}(1)(0.2c_w\sin(\beta))\right] \end{pmatrix} \tag{6}$$

$$\mathbf{U}_{cp} = \begin{pmatrix} \rho|\nu|\nu D_p^4(C_{t0_p} + C_{t1_p}J_p + C_{t2_p}J_p^2 + C_{t3_p}J_p^3) \\ -\rho|\nu|D_p^3 w C_n \\ -\rho|\nu|\nu D_p^5(C_{q0_p} + C_{q1_p}J_p + C_{q2_p}J_p^2 + C_{q3_p}J_p^3) \end{pmatrix}. \tag{7}$$

where c_w, b_w, S_w, d_{aw} are some geometrical characteristics of the wings, and ρ is the sea water density. A set of numerical values of the above coefficients can be found in Appendix section A. Such a model, which is not unique, can vary depending on design.

Some features are worthy of comment in connection with this model :

- The AUV state equations split rather naturally into two subsets reflecting the evolution of the local variables (u,w,q) and of the absolute variables (x_c,z_c,θ_c).
- For a neutrally buoyant vessel, the gravity term $\mathbf{\Gamma}_g$ is zero.
- The AUV is a nonlinear system but the nonlinearities primarily consist of bilinear terms in the local state variables plus sinusoidal-type nonlinearities in the control matrices and the absolute coordinates.
- The range of achievable control vector values, $\mathbf{U}_{cp}+\mathbf{U}_{cw}$, is limited. This indicates the inability of this type of AUV to accelerate in an arbitrary direction (such as only orthogonal to the long axis). Such constraints on the dynamics are akin to nonholonomy.
- The response of the AUV to a positive step change in the wings turning, β, is initially to accelerate w in the opposite direction causing an initial decrease in z_c in order to gain an eventual increase. This behaviour is reminiscent of nonminimum-phase systems.

These last two observations would suggest not to attempt to use a feedback control strategy which relies on high-gain or on system inversion.

3 Control Problem

3.1 Formulation

As indicated above, our aim is to design a controller to permit the AUV to follow an *a priori* unknown ocean floor at a fixed distance. The formal specification of the *Task* for a system (and robotic mechanisms in particular) is a central factor in developing a control solution [Slotine and Li, 1991]. This includes the selection of appropriate output and performance measurement functions. For our problem we take, in the first instance, as our output the orthogonal distance (or altitude), y, of the AUV from the ocean floor. It is shown further that y is the minimal information that is required for a good enough behavior of the controller. This output variable is a function of the evolution of the ocean floor in addition to that of the AUV. This is depicted in Figure 1. Indeed, y partly describes the interaction of the AUV with its environment. We define the following new variables :

$(x^\star(t), z^\star(t))$ the coordinates in the absolute frame of the point on the ocean floor closest to the AUV. Thus :

$$y(t) = \left((x_c(t) - x^\star(t))^2 + (z_c(t) - z^\star(t))^2\right)^{\frac{1}{2}} sign(z^\star(t) - z_c(t))$$

$\theta^\star(t)$ the slope of the ocean floor at $(x^\star(t), z^\star(t))$ as measured relative to the absolute frame. Thus taking into account the specific angle notations for AUVs :

$$\theta^\star(t) = -\tan^{-1}\left(\left.\frac{dz^\star}{dx^\star}\right|_{(x^\star(t),z^\star(t))}\right)$$

$\theta(t)$ the orientation of the AUV relative to the bottom :

$$\theta(t) \triangleq \theta_c(t) - \theta^\star(t) \tag{8}$$

We commence with the control objective of having the AUV follow the bottom without regard to the nature or speed of the variation of the bottom. We also limit our consideration to the use of the wings angle, β, as the single control variable to achieve this objective. In line with standard formulations of predictive control, we choose a quadratic performance criterion :

$$J \triangleq \lim_{T\to\infty} \frac{1}{T}\int_0^T \left[y(t)^2 + \lambda\beta(t)^2\right] dt, \tag{9}$$

where λ is a penalty on the control action.

Remarks :

- u_0^2 may be introduced as a penalty on the altitude variable y in (9) in order to have the trajectory less dependent on u_0 values, as already done in [Santos et al., 1995b].
- Penalizing the control action, i.e. increasing λ, means to decrease the AUV reactivity and ability to converge to the desired bottom following, however a possible benefit is lower resulting altitude deviations due to lower control actions. It has been proven through simulations that, for linear profiles, decreasing the control action penalty does not always correspond to lower altitude deviations, however that, for parabolic and sinusoidal profiles, the lower the control penalty is, the lower the altitude deviations are, while remaining within the convergence domain.

It is clear that (9) embodies a tracking control problem. However, without prior knowledge of the bottom $z^\star = h_f(x^\star, t)$, it is not useful to develop this line. Rather, we pose the problem as one of *disturbance rejection* in which the evolution of the bottom is treated as perturbation to the process output y. (In this way, we actually remain close to the formulations of predictive control in the process industries and further can benefit from existing design principles.)

3.2 The Linearized Model

We derive a linearized model of the AUV for use in developing control laws. To do this, we assume that the axial velocity, u, is constant. This is a reasonable assumption since the task of bottom following will typically require a nominal constant value, u_0, of u that is generally imposed by the technical specifications of the load sensor. Further, since this is primarily the concern of the ν control signal, the regulation of u can be separated from the regulation of the other variables, which focuses on the use of β to permit following the bottom.

We take as our linearized model the w and q components of (1), yielding :

$$\mathbf{M}_I^p \begin{pmatrix} \dot{w}(t) \\ \dot{q}(t) \end{pmatrix} = u_0 \begin{pmatrix} C_{zw} & C_{zq}+m \\ C_{mw} & C_{mq} \end{pmatrix} \begin{pmatrix} w \\ q \end{pmatrix} + \begin{pmatrix} \gamma_1 \\ \gamma_2 \end{pmatrix} \beta(t). \tag{10}$$

Here the parameters C_{zw},... are elements from the drag matrix $\mathbf{D}_h$, while the additional term m in the (1,2) position comes from the Coriolis term. $\mathbf{M}_I^p$ is the subset of the inertia matrix $\mathbf{M}$ that is restricted to state variables (w,q). The elements γ_1 and γ_2 are linearized from (6) :

$$\begin{aligned} \gamma_1 &= -0.5\rho S_w V^2 \left[C_{zow} - C_{xow}\right] \\ \gamma_2 &= 0.5\rho S_w V^2 \left[d_{aw}(C_{zow} - C_{xow}) - 0.2 c_w C_{zow}\right] \end{aligned}$$

The interaction of the AUV with the environment is modelled by considering θ from (8). The output measurement of the AUV is related to these variables as follows, assuming that the followed bottom curve is at least $\mathcal{C}^1$:

$$\dot{y}(t) = u\sin(\theta) - w\cos(\theta) \tag{11}$$

which we may linearize about θ=0 as :

$$\dot{y}(t) = u\theta - w. \tag{12}$$

The behaviour of the ocean floor is included into the modelling phase by re-writing the derivative of θ to include the evolution of the bottom :

$$\begin{aligned} \dot{\theta}(t) &\triangleq \dot{\theta}_c(t) - \dot{\theta}^\star(t) \\ &= q(t) + f(t). \end{aligned} \tag{13}$$

This equation defines the function f which is clearly related to the changing slope of the bottom to be followed. A novelty of our approach is to include this signal as a disturbance to the AUV and to use the design tools of disturbance rejection to effect a controller. Since the disturbance $f(t)$ is not measured ahead of time, we need to use a model to describe its evolution or, at least, the evolution of that part of it which we seek to reject. For this, we take a linear lowpass model :

$$\dot{x}_f(t) = A_f x_f(t) + B_f \xi(t), \quad f(t) = C_f x_f(t), \tag{14}$$

where $\xi(t)$ is white noise. To reflect the distinction between the comportment of the model state $y(t)$ and the measured output, we denote the former as $k(t)$.

Our total linear model then has the form,

$$\begin{pmatrix} \dot{w}(t) \\ \dot{q}(t) \\ \dot{\theta}(t) \\ \dot{k}(t) \\ \dot{x}_f(t) \end{pmatrix} = \begin{pmatrix} a_{11} & a_{12} & 0 & 0 & 0 \\ a_{21} & a_{22} & 0 & 0 & 0 \\ 0 & 1 & 0 & 0 & C_f \\ -1 & 0 & u & 0 & 0 \\ 0 & 0 & 0 & 0 & A_f \end{pmatrix} \begin{pmatrix} w(t) \\ q(t) \\ \theta(t) \\ k(t) \\ x_f(t) \end{pmatrix} + \begin{pmatrix} \gamma_1 \\ \gamma_2 \\ 0 \\ 0 \\ 0 \end{pmatrix} \beta(t) + \begin{pmatrix} 0 \\ 0 \\ 0 \\ 0 \\ B_f \end{pmatrix} \xi(t) \quad (15)$$

$$y(t) = \begin{pmatrix} 0 & 0 & 0 & 1 & 0 \end{pmatrix} \begin{pmatrix} w(t) \\ q(t) \\ \theta(t) \\ k(t) \\ x_f(t) \end{pmatrix} + \eta(t), \quad (16)$$

where $\eta(t)$ is measurement noise.

At this moment, some remarks should be done :

- Tests show that w cannot be neglected, and singular perturbation approach cannot be applied to this type of AUV model, at least where high performance tracking is needed.
- It is evident from (15–16) that $k(t)$ can be seen at a first instance as an integration of $\theta(t)$, and $\theta(t)$ as an integration of $q(t)$. Indeed, when x_f and w are near zero (i.e. respectively no bottom variation and few vertical skidding effect), the above linearized model becomes :

$$\begin{aligned} \dot{q}(t) &= a_{22}q(t) + \gamma_2\beta(t) \\ \dot{\theta}(t) &= q(t) \\ \dot{k}(t) &= u_0\theta(t) \\ y(t) &= k(t) \end{aligned}$$

  This justifies our choice of y as a minimal information we need for a convenient control design.

Our linearized control formulation is to seek to minimize the performance criterion J of (9) subject to y being generated by the model (15–16). This is a standard LQG disturbance rejection problem in which f acts as a disturbance process. Its solution will be given by standard linear state-variable feedback plus state estimation via a Kalman filter. We shall investigate the design issues of this in the next section[1].

[1] One feature worth remarking upon is that this linear model, arrived at by assuming u fixed, might be unstable even though the AUV without control is dissipative. This is due to the artificial suppression of the Coriolis term from w to u, which is part of the stabilizing action.

4 LQG Control Design

4.1 Formulation

Our formulation of a linear model (15–16) which links the AUV steering input $\beta(t)$ to the measured distance from the ocean floor $y(t)$ permits the posing and solution of a Linear Quadratic Gaussian (LQG) controller which may be applied in feedback on the nonlinear AUV system (1–2). We proceed by writing (15–16) as :

$$\begin{aligned} \dot{\mathbf{x}}(t) &= \boldsymbol{\mathcal{A}}\mathbf{x}(t) + \boldsymbol{\mathcal{B}}\beta(t) + \boldsymbol{\zeta(t)} && (17) \\ y(t) &= \boldsymbol{\mathcal{C}}\mathbf{x}(t) + \eta(t), && (18) \end{aligned}$$

where $\boldsymbol{\zeta}$ and η are independent zero-mean gaussian white noise processes with variances $\boldsymbol{\mathcal{Q}_o}$ and $\mathcal{R}_o$ respectively, and taking the LQ performance objective as :

$$J \triangleq \lim_{T\to\infty} \frac{1}{T} \int_0^T \left[\mathbf{x}^T(t)\boldsymbol{\mathcal{Q}_c}\mathbf{x}(t) + \beta^T(t)\mathcal{R}_c\beta(t)\right] dt$$

The LQG controller is composed of a linear state estimator (Kalman filter) followed by linear state-variable feedback :

$$\begin{aligned} \dot{\hat{\mathbf{x}}}(t) &= (\boldsymbol{\mathcal{A}} - \boldsymbol{\mathcal{M}}\boldsymbol{\mathcal{C}} + \boldsymbol{\mathcal{B}}\boldsymbol{\mathcal{K}})\,\hat{\mathbf{x}}(t) + \boldsymbol{\mathcal{M}}y(t) && (19) \\ \beta(t) &= \boldsymbol{\mathcal{K}}\hat{\mathbf{x}}(t), && (20) \end{aligned}$$

where $\hat{\mathbf{x}}(t)$ is an estimate of the state of the linearized model and the gains $\boldsymbol{\mathcal{K}}$ and $\boldsymbol{\mathcal{M}}$ are computed from the respective algebraic Riccati equations :

$$\begin{aligned} \mathbf{0} &= \boldsymbol{\mathcal{A}}^T\boldsymbol{\mathcal{P}} + \boldsymbol{\mathcal{P}}\boldsymbol{\mathcal{A}} - \boldsymbol{\mathcal{P}}\boldsymbol{\mathcal{B}}\mathcal{R}_c^{-1}\boldsymbol{\mathcal{B}}^T\boldsymbol{\mathcal{P}} + \boldsymbol{\mathcal{Q}_c} && (21) \\ \boldsymbol{\mathcal{K}} &= -\mathcal{R}_c^{-1}\boldsymbol{\mathcal{B}}^T\boldsymbol{\mathcal{P}} && (22) \\ \mathbf{0} &= \boldsymbol{\mathcal{A}}\boldsymbol{\mathcal{S}} + \boldsymbol{\mathcal{S}}\boldsymbol{\mathcal{A}}^T - \boldsymbol{\mathcal{S}}\boldsymbol{\mathcal{C}}^T\mathcal{R}_o^{-1}\boldsymbol{\mathcal{C}}\boldsymbol{\mathcal{S}} + \boldsymbol{\mathcal{Q}_o} && (23) \\ \boldsymbol{\mathcal{M}} &= \boldsymbol{\mathcal{S}}\boldsymbol{\mathcal{C}}^T\mathcal{R}_o^{-1} && (24) \end{aligned}$$

4.2 Linear Design Capabilities

The design aspects of LQG control move from the selection of controller parameters to the selection of criteria to be optimized. That is, the design takes place through the manipulation of the weightings $\boldsymbol{\mathcal{Q}_o}$, $\mathcal{R}_o$, $\boldsymbol{\mathcal{Q}_c}$, $\mathcal{R}_c$ of the optimization. The resulting LQG controller (19–20) is a dynamical system which has input $y(t)$ and output $\beta(t)$. It may be applied directly to the nonlinear AUV as a feedback controller, although questions of its suitability must arise because of its simplification. Indeed the major issue is one of robustness of the controller performance to linearization errors together with the tuning of the linear controller to achieve better nominal performance.

One approach to improving (or at least manipulating) controller robustness margins and closed loop performance is *Loop Shaping* [Doyle et al., 1992] or *Frequency-Weighting*. In the case of LQG control, Frequency-Weighting consists principally in replacing the penalty matrices $\mathcal{Q}_c$ and $\mathcal{R}_c$ by transfer functions whose amplitude varies with frequency. This alters the frequency distribution of the cost, increases the controller order and also adds filters into the closed loop as will be illustrated in the example shortly.

At this stage, we have identified three modes to vary the properties of the linear controller designed by LQG methods with the linearized model above :

- modification of the weighting matrices $\mathcal{Q}_o$, $\mathcal{R}_o$, $\mathcal{Q}_c$, $\mathcal{R}_c$, (As is evident from the LQ criterion, the relative sizes of $\mathcal{Q}$ and $\mathcal{R}$ are the important factor for linear design.)
- frequency-weighting of the matrices $\mathcal{Q}_c$, $\mathcal{R}_c$ in the LQ design to effect loop shaping and/or signal filtering,
- selection of the disturbance model $[A_f, B_f, C_f]$ associated with the statistical description of the evolution of the ocean floor. Referring to the model disturbance (14), the parameters tuning can be reduced to that of $[A_f, B_f]$ with $C_f = -A_f$, as its gain is $C_f B_f / A_f$ and its pole A_f.

There is a close connection between the latter two design approaches [SANDF].

We note that the linear LQG controllers developed so far have been generated as variations on the theme of standard infinite-horizon LQG methods. We remind the reader here that we might equally have selected receding-horizon or finite-horizon criteria in order that the approach be directly interpreted as a predictive controller. The distinction in the realm of linear controllers is not great but, with the introduction of constraints and other nonlinearities, the predictive control formulation has distinct feasibility advantages [Michalska and Mayne, 1993], where the control signal is derived via explicit open-loop optimization.

5 Linear Control Design and Performance with the AUV

5.1 Linear Control Design — LQG/LTR

The bottom-following control objective (9) is associated with the following choices of LQ design parameters :

$$\mathcal{Q}_c = \mathcal{C}^T \mathcal{C}, \quad \mathcal{R}_c = \sigma$$

Similarly, the noise processes $\boldsymbol{\zeta}$ and η of (17–18) are given as functions of ξ and η of (15–16) to yield Kalman filter design parameters :

$$\boldsymbol{\mathcal{Q}_o} = \boldsymbol{\mathcal{G}}\boldsymbol{\mathcal{G}}^T, \quad \mathcal{R}_o = \kappa$$

where $\boldsymbol{\mathcal{G}}$ is the matrix multiplier of ξ in (15).

With these selections of design parameters, one may proceed to complete the LQG design taking κ and σ as the (scalar) design parameters. However, given the admitted approximation made in taking the linearized model, it is prudent to consider a slightly different approach with some stability robustness guarantees — LQG with Loop Transfer Recovery (LTR). The LTR design attempts to preserve the robustness margin of either the LQ design with full state feedback or the Kalman filter with open-loop control. The sacrifice in this approach is the optimality of the LQG solution. But, since the optimization criterion is used primarily as a design tool, this is not a severe compromise.

The disturbance rejection formulation of (17–18) yields a state-space model (17) which is not completely controllable. The state of the disturbance process, x_f, clearly is not accessible by the control. Accordingly, robust closed-loop stability needs to devolve primarily from the weighting associated with the AUV states. At the centre of LTR is the selection of the Kalman filter weightings dual to those of the LQ design, which is effected by modelling the state noise as entering the open-loop system through the input channel. Thus we select :

$$\boldsymbol{\mathcal{Q}_o} = \boldsymbol{\mathcal{B}}\boldsymbol{\mathcal{B}}^T + \boldsymbol{\mathcal{G}}\boldsymbol{\mathcal{G}}^T, \quad \mathcal{R}_o = \kappa$$

with κ taken as small as is feasible for good performance. An equivalent alternative approach to loop transfer recovery is to let σ be as small as is feasible. See for example [Anderson and Moore, 1990] for a fuller treatment of LQG robust stability.

An advantage of the above LQG/LTR approach is that it maintains the low number of free variables of the design, so that only σ and κ need to be chosen once the disturbance model is fixed. Later, we shall also see that the LTR method also coincides with sensible selections of design parameters from a nonlinear robustness viewpoint. We shall next explore the performance of this linear control design with the nonlinear AUV.

In Figure 2, the frequency response magnitudes are displayed for a sequence of LQG design for the AUV controller, when having the controller parameters values varied. One may discern the anticipated effect on the control action and the effects of the variation of parameters on the resulting controller.

5.2 Linear Control Performance in Tracking

Tests have been conducted considering three types of bottom profile : inclined line, parabolic curve and an ascending periodic curve. In every case, the vehicle

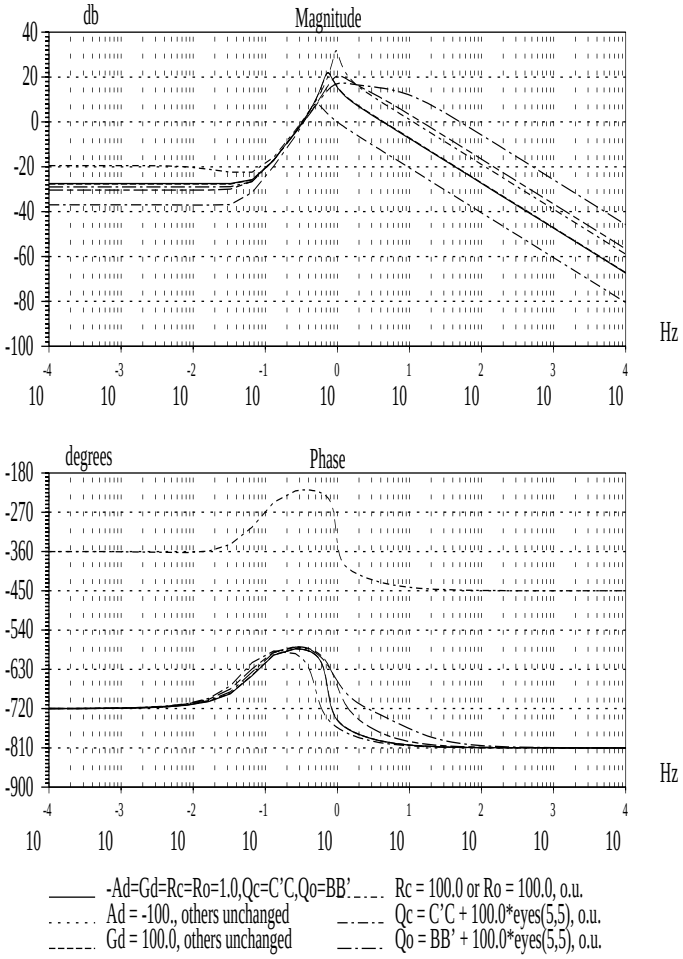

Figure 2: Magnitude frequency responses for LQG/LTR controller with various parameters values.

initial orientation $\theta_c(0)$ and initial altitude $(y(0))$ are zero. The vehicle is initiated with an initial advancement velocity $u_0 = 2m/sec$, that is maintained during the simulation. Same tests with advancement velocity of $1m/sec$ and $3m/sec$ can be found in Appendix section C.

Considering the results obtained in the conditions described above, and that are depicted in Figures 3,4,5 (each of them includes eight charts numbered from (a) to (h)), some conclusions can be done :

- The AUV, as actuated with rear wings, is obviously a nonminimum phase system as can be seen on charts (b) from each type of bottom simulation. Indeed, to join an upper point of the bottom, the vehicle begins by descending before ascending.

- The control signal input on charts (h) is highly chattered. Furthermore, various simulations on the variation of the vehicle actuators nonlinearities emphasize that the higher these nonlinearities are, the higher the induced chattering effects are. This is due to the chattered estimations of AUV variables w and q (charts (c) and (d)) using the linearized model (15). This phenomenon is worst when the initial vehicle situation (z_c, θ_c) is far from the desired one, and it decreases near convergence. It can be explained as a direct consequence of the sinusoidal terms appearing in the AUV and, more, in its actuators dynamics, and that are neglected in the linearized model.

- The skidding effects are not negligible as can be seen on charts (b). The maximum altitude value varies considerably depending on bottom profile characteristics and variation, initial AUV-bottom configuration, and of course controller parameters. On this last point, it is worth noticing that the fine tuning of controller parameters is significant, and does interact with previously cited variables. Care must be paid to these bad effects in order to avoid collision when servoing too close from a bottom (e.g for camera surveys at $y_d \approx 5m$).

- $\hat{f}$, the estimation of the bottom orientation variation, mainly depends on the G_d parameter : G_d should be lowered for non-varying bottom, while increased for varying bottom orientation. Therefore, G_d can be viewed as related to the energy in the external disturbance.

- Comparing the simulation results for various advancement velocities (Figures 12,14,16 for $u_0 = 1m/sec$, Figures 3,4,5 for $u_0 = 2m/sec$, Figures 18,20,22 for $u_0 = 3m/sec$), it appears that, the time of convergence is shorter for increasing velocities, while the control actions are lowered. This is due to the better increasing efficiency of mobile wings in this range of speed. It is worth noticing that the maximal altitude deviations

remain the same, meaning that the altitude maximal deviations are not dependent on the axial advancement velocity.

- Saturations on wings turning do not prevent from converging thanks to a convenient choice of controller parameters, as depicted on Figures 24–26.
- Further simulations (e.g. in Figure 32) show that the controller does no more ensure convergence when facing high structured uncertainties on hydrodynamic coefficients in conjunction with a varying bottom profile.

There is no guarantee that a set of controller parameters can be found that lead to "optimal" response as, at the origin of the approach, a physical normalization is required between input (wings turning in radian unit) and output (altitude in meter unit). Optimality is machine- and application-dependent.

5.3 Frequency-weighted LQG Design

The aim in controlling the AUV to follow the changes in ocean floor profile is to respond to those changes which represent systematic, long-term variations of the bottom without responding to small-scale local variations. This can partially be accommodated through the selection of the disturbance model, regarding other out-of-band signals as white noise. A more direct manner to effect this response is to alter the LQ criterion so that high-frequencies in the measured output, $y(t)$, are penalized less than low-frequencies. Further, by increasing the penalty on high-frequency control actions, smoother responses can be achieved.

We introduce the frequency-weightings to our design by posing a modified LQ criterion :

$$J_{FW} = \lim_{T\to\infty} \frac{1}{T} \int_0^T \left[(F_1(z)y(t))^2 + \lambda (F_2(z)\beta(t))^2 \right] dt, \tag{25}$$

where F_1 is a low-pass minimum-phase filter and F_2 is a high-pass minimum-phase filter. The notation of (25) means that a model must be constructed in which the signals of $y(t)$ filtered through the transfer function $F_1(z)$ and $\beta(t)$ filtered through $F_2(z)$ are available and are used in the minimization of this LQ criterion. Thus these filters add extra order to the resulting feedback controller.

If we denote by $P(z)$ the process model — here the linearized AUV dynamics from β to y — and by $H(z)$ the disturbance process — here the transfer function between ξ and y — then the frequency weighted LQG problem has a feedback controller given by $C_{FW} = F_2^{-1} F_1 \bar{C}$ where $\bar{C}$ is the LQG controller for the disturbance rejection problem with process model $P F_2^{-1} F_1$ and disturbance process $F_1 H$. Thus the frequency weighting can be seen to implement directly a filtering $F_2^{-1} F_1$ into the feedback path which, in the case of

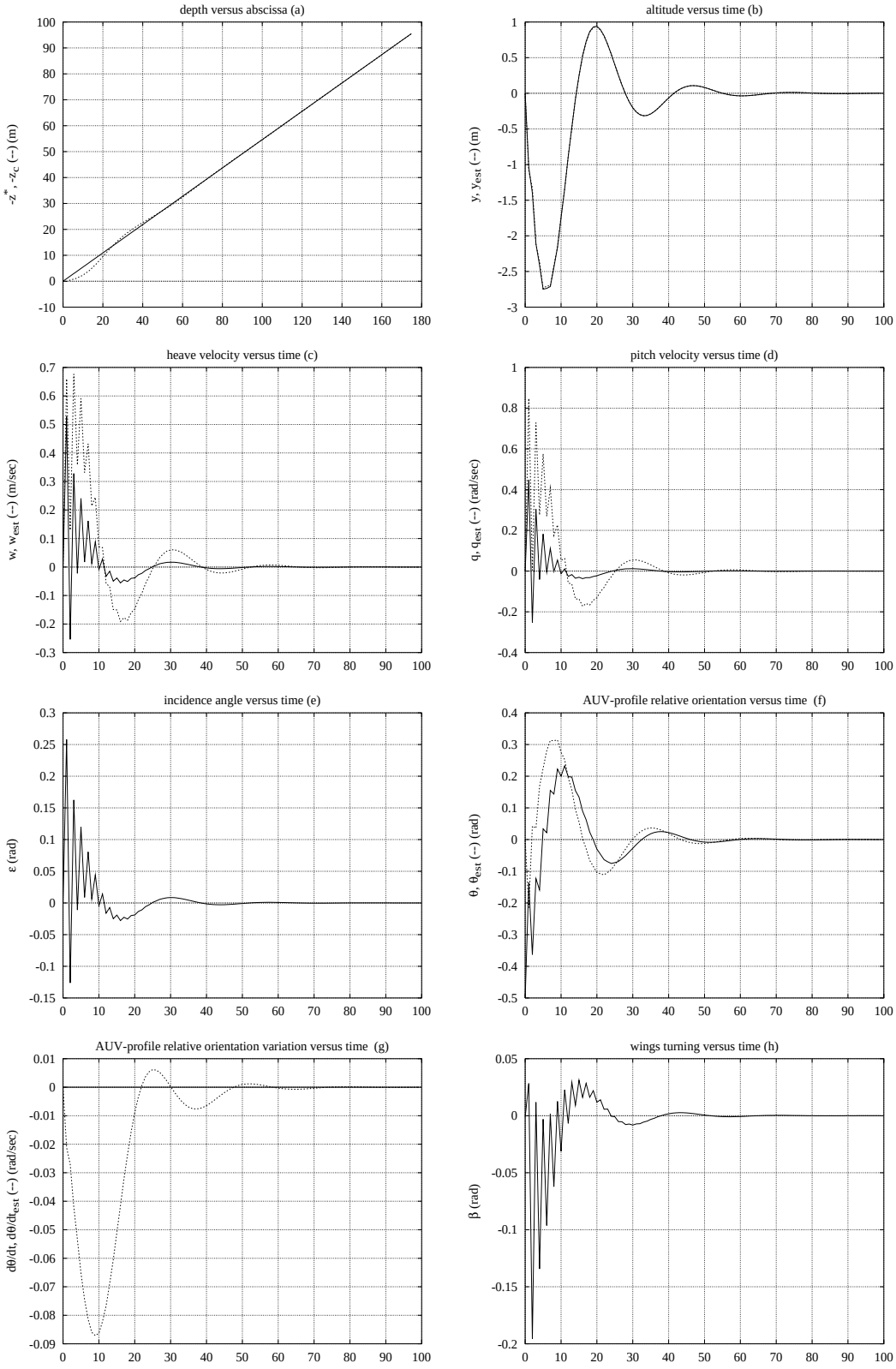

Figure 3: Simulation on linear bottom profile using the LQG/LTR linear controller. Main parameters value : bottom slope=0.5rad, vehicle initial orientation=0rad, Rc=30.0, Ro=0.1, Ad=-.1, Cd=-Ad, Gd=5.0

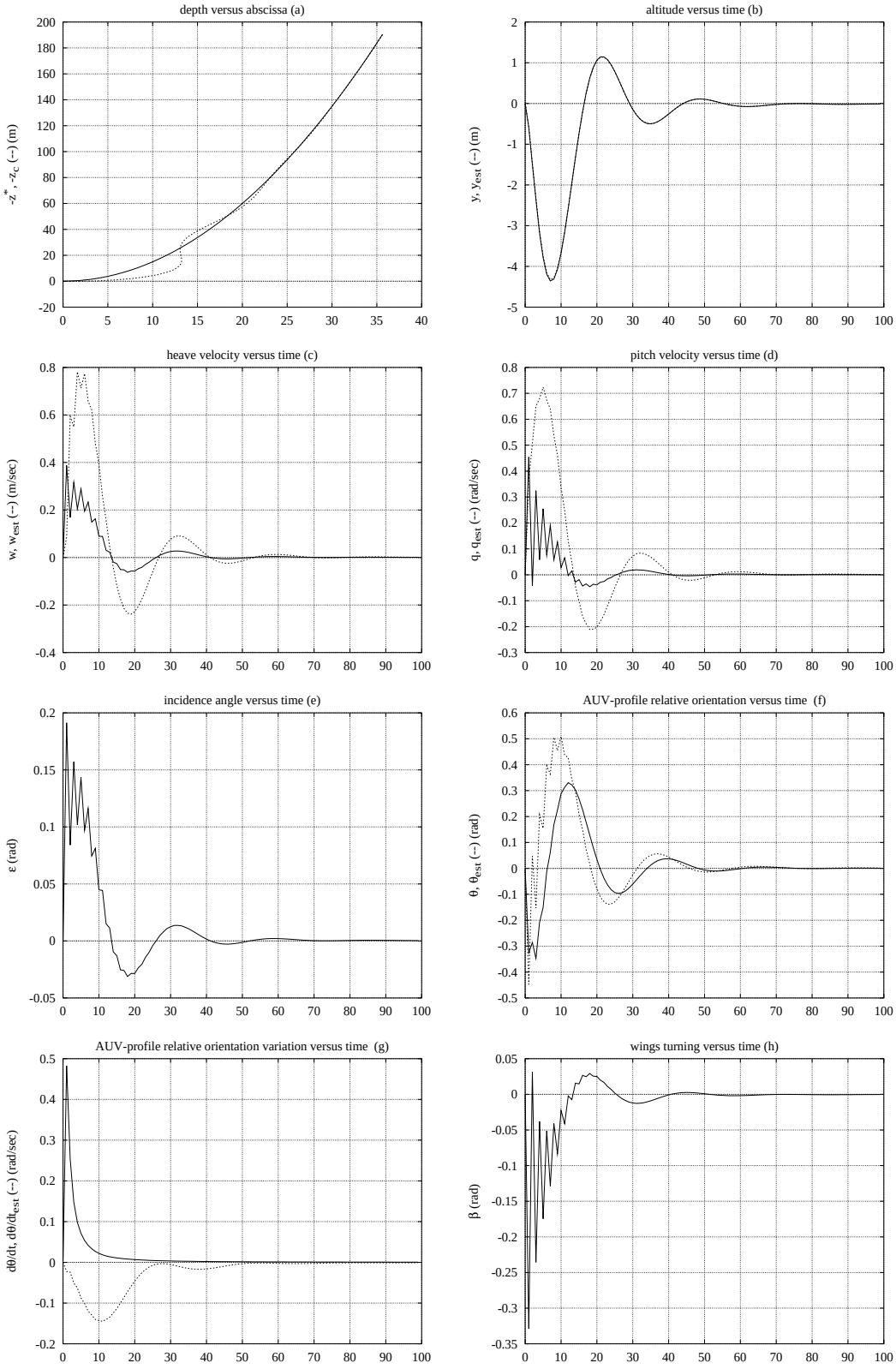

Figure 4: Simulation on parabolic bottom profile using the LQG/LTR controller. Main parameters value : bottom : $z^* = -0.15x^{*^2} + z0$, vehicle initial orientation=0rad, Rc=30.0, Ro=0.1, Ad=-.1, Cd=-Ad, Gd=5.0

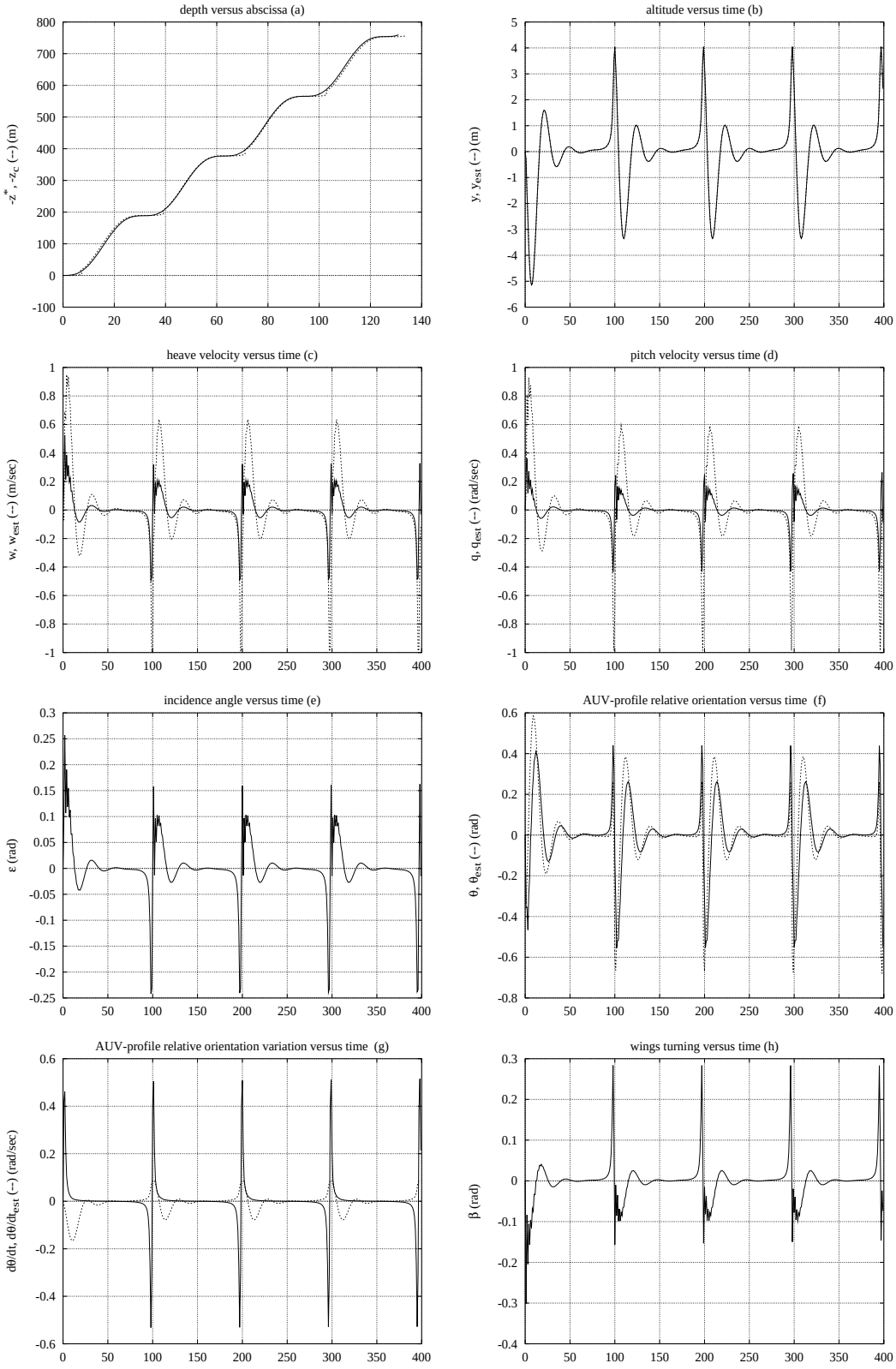

Figure 5: Simulation on "quasi" sinusoidal bottom profile using the LQG/LTR controller. Main parameters value : bottom period : $\approx 100sec$, vehicle initial orientation=0rad, Rc=30.0, Ro=0.1, Ad=-.1, Cd=-Ad, Gd=5.0

low-pass F_1 and high-pass F_2 yields the expected rejection of high-frequency measurements, without upsetting the stability of the nominal model. In addition to these performance benefits of frequency-weighting, the approach is also central to the design and management of design stability robustness, [Anderson and Moore, 1990]. The methodology with emphasis on the AUV is detailed in Appendix section B.

In Figure 6, the frequency response magnitudes are displayed for a sequence of frequency-weighted LQG design for the AUV controller. The penalties are as outlined above, i.e. F_1 low-pass and F_2 high-pass (here using simple lead-lag network filters), with basic configurations with cutoff frequency at 0.01Hz and with gain variation between pass- and stop-bands of 1 through to 100. One may discern the anticipated effect on the control action and the effects of the variation of filters parameters on the resulting controller, and compare with Figure 2.

6 Nonlinear Control Design

It is evident from the simulation experiments of earlier sections, that a linearized LQG/LTR controller can perform quite well in the AUV bottom tracking problem. Further, it should also be evident that these linear designs contain a great capacity for simple design variation via costing selection which is logically tied to the achievement of control or mission objectives. Our task in this section will be to migrate or translate this linear methodology into the nonlinear framework to yield more highly performing controller which are cognisant of the AUV nonlinearities but which preserve the access to the linear design tools.

6.1 Extended Kalman filter incorporation

From the earlier simulation experiments, it is evident that a cause of poor control performance of the AUV tracker is due to the misalignment between the state of the (nonlinearly evolving) AUV and the linearly evolving state estimate contained in the controller. Indeed, because the state variables have been retained with their physical meaning, it is possible to study the quality of estimation of the state and to infer the consequent degradation of control outcome. It is clear that $k(t)$ is well estimated, while progressively θ, q and w concur more poorly, as seen in Figures 3, 4, and 5. Given that the nonlinearities of the control signal and of the output evolution have been suppressed, better estimation of the state might be expected from including these into the estimator design. This, in effect, leads to the adoption of an extended Kalman filter (EKF).

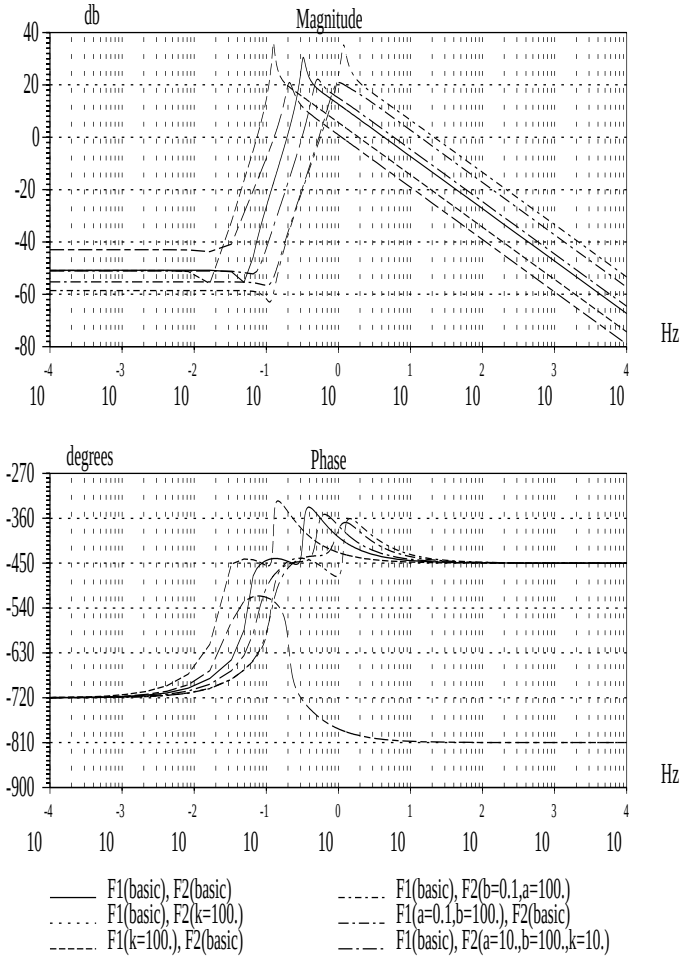

Figure 6: Magnitude frequency responses for frequency-weighted LQG controllers. The form of the filters is a first-order simple lead-lag network : F(s) = k(1+s/a)/(1+s/b). For the low-pass filter F1, the basic configuration has the following values : k=1.0, a=1.0, b=0.01 . For the high-pass filter F2, the basic configuration has the following values : k=1.0, a=0.01, b=1.0 .

In the EKF, the nonlinear state evolution of (1) is retained together with the evolution of the output variable y of (11) to yield a nonlinear estimator of the form :

$$\begin{pmatrix} \dot{\hat{w}}(t) \\ \dot{\hat{q}}(t) \\ \dot{\hat{\theta}}(t) \\ \dot{\hat{x}}_f(t) \end{pmatrix} = \begin{pmatrix} a_{11} & a_{12} & 0 & 0 \\ a_{21} & a_{22} & 0 & 0 \\ 0 & 1 & 0 & C_f \\ 0 & 0 & 0 & A_f \end{pmatrix} \begin{pmatrix} w(t) \\ q(t) \\ \theta(t) \\ x_f(t) \end{pmatrix} + \begin{pmatrix} \mathbf{U}_{cw}^{[2]}(t) \\ \mathbf{U}_{cw}^{[3]}(t) \\ 0 \\ 0 \end{pmatrix} + \boldsymbol{\mathcal{M}}_1(y(t) - \hat{y}(t)) \quad (26)$$

$$\dot{\hat{k}}(t) = u_0 \sin(\hat{\theta}(t)) - \hat{w}(t)\cos(\hat{\theta}(t)) + \boldsymbol{\mathcal{M}}_2(y(t) - \hat{y}(t)) \quad (27)$$

$$\hat{y}(t) = \hat{k}(t), \quad (28)$$

where $\boldsymbol{\mathcal{M}}_1$ and $\boldsymbol{\mathcal{M}}_2$ are submatrices of the Kalman filter gain $\boldsymbol{\mathcal{M}}$, containing block rows (1,2,3,5) and 4, respectively, and $\mathbf{U}_{cw}^{[2]}$ and $\mathbf{U}_{cw}^{[3]}$ are the second and third components of the nonlinear driving terms from (6).

We note that this is not the complete EKF, since the Kalman gain matrix, $\boldsymbol{\mathcal{M}}$, is computed using a fixed linearization of the AUV dynamics. A full EKF would use the local linearizations about current predicted and filtered state estimates to compute $\boldsymbol{\mathcal{M}}$. The inclusion of the other nonlinear aspects of state and output evolution do however derive from the EKF and are incorporated to provide more reliable state estimates. The design aspects of EKFs reflect basically those of the Kalman filter with some modifications. Most notably, in order to obtain an EKF which incorporates some robustness to linearization errors, it is necessary to use a value of $\boldsymbol{\mathcal{Q}_o}$ which is larger than the value corresponding to the actual state noise variance entering the state recursion in the nonlinear case [LaScala et al., 1995]. Given that, we have chosen to use a variant of LQG/LTR in the design of the linear controller that employs a reduced value of $\mathcal{R}_o$. Indeed, we have already chosen a strategy which is consistent with this objective, since increasing $\boldsymbol{\mathcal{Q}_o}$ in the linear design is equivalent to decreasing $\mathcal{R}_o$.

6.2 EKF plus LQ feedback control — simulation results

Allied with the nonlinear state estimation yielding the estimate $\hat{x}(t)$, the control calculation remains fixed as linear state-variable estimate feedback given by (20) :

$$\beta(t) = \boldsymbol{\mathcal{K}}\hat{\mathbf{x}}(t)$$

That is, the LQ control law remains unchanged from the fully linear version and only the estimation part is altered. This is a partial nonlinearization of the previous control regime. As can be seen when comparing results on Figures 7,8,9 respectively with those on Figures 3,4,5, for identical controller parameters, bottom profile and AUV initial situation, there are real improvements on the bottom profile following. Indeed, :

- As can be seen on charts (b) from each type of bottom simulation, the time for convergence is much shorter (approximately three times). Furthermore, the maximal altitude from skidding effects is at least reduced by half.

- The control signal input on charts (h) is no more highly chattered. This is due to the better estimations of AUV variables w and q (charts (c) and (d)) using the nonlinear estimator (26–28).

- There is a lesser deviation of $\hat{f}$, the estimation of the bottom orientation variation (chart (g)), which then fits better the real value.

- Comparing the simulation results for various advancement velocities (Figures 13,15,17 for $u_0 = 1m/sec$, Figures 7,8,9 for $u_0 = 2m/sec$, Figures 19,21,23 for $u_0 = 3m/sec$), it appears that, the time of convergence is shorter for increasing velocities, while the control actions are lowered. This is due to the better increasing efficiency of mobile wings in this range of speed. It is worth noticing that the maximal altitude deviations remain the same, meaning that the altitude maximal deviations are not dependent on the axial advancement velocity. Furthermore, if compared to the strictly LQG/LTR linear controller results obtained at identical velocities, the resulting control actions are much lowered.

- For various initial conditions ($(y(0), \theta(0)) \neq (0, 0)$), the LQG/LTR+EKF controller behaves much better with shorter time of convergence, better state estimation, and mainly significant lesser maximum altitude deviations (see Figures 28–31).

- As for LQG/LTR controller, saturations on wings turning do not prevent from converging thanks to a convenient choice of controller parameters, as depicted on Figures 25–27.

- Further simulations (see Figure 33) show that the controller is robust with respect to uncertainties on hydrodynamic coefficients, with significant better results on altitude deviations and state estimates, if compared to linear LQG/LTR controller resulting action (see Figure 32).

These simulations have been conducted with full EKF, computing $\mathcal{M}$ at each iteration. When compared to some simulations using constant $\mathcal{M}$, there is no significant improvement in the results.

6.3 Fully nonlinear design

Our approach so far has been to develop the feedback control law from the basis of the linear LQG (or frequency-weighted LQG) methods. In this way,

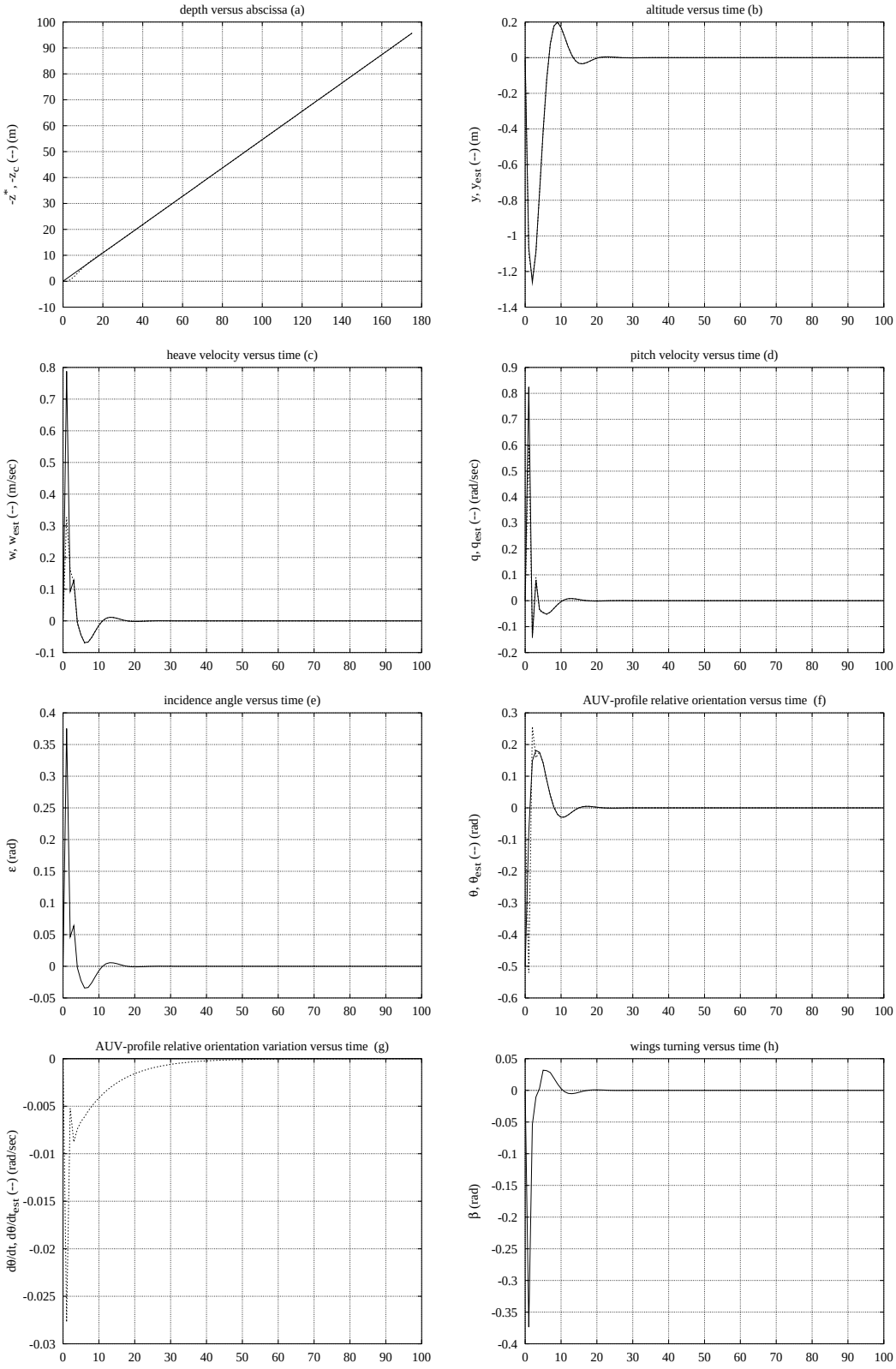

Figure 7: Simulation on linear bottom profile using the LQG/LTR+EKF controller. Main parameters value : bottom slope=0.5rad, vehicle initial orientation=0rad, Rc=30.0, Ro=0.1, Ad=-.1, Cd=-Ad, Gd=5.0 (identical to those for simulations using LQG/LTR controller before)

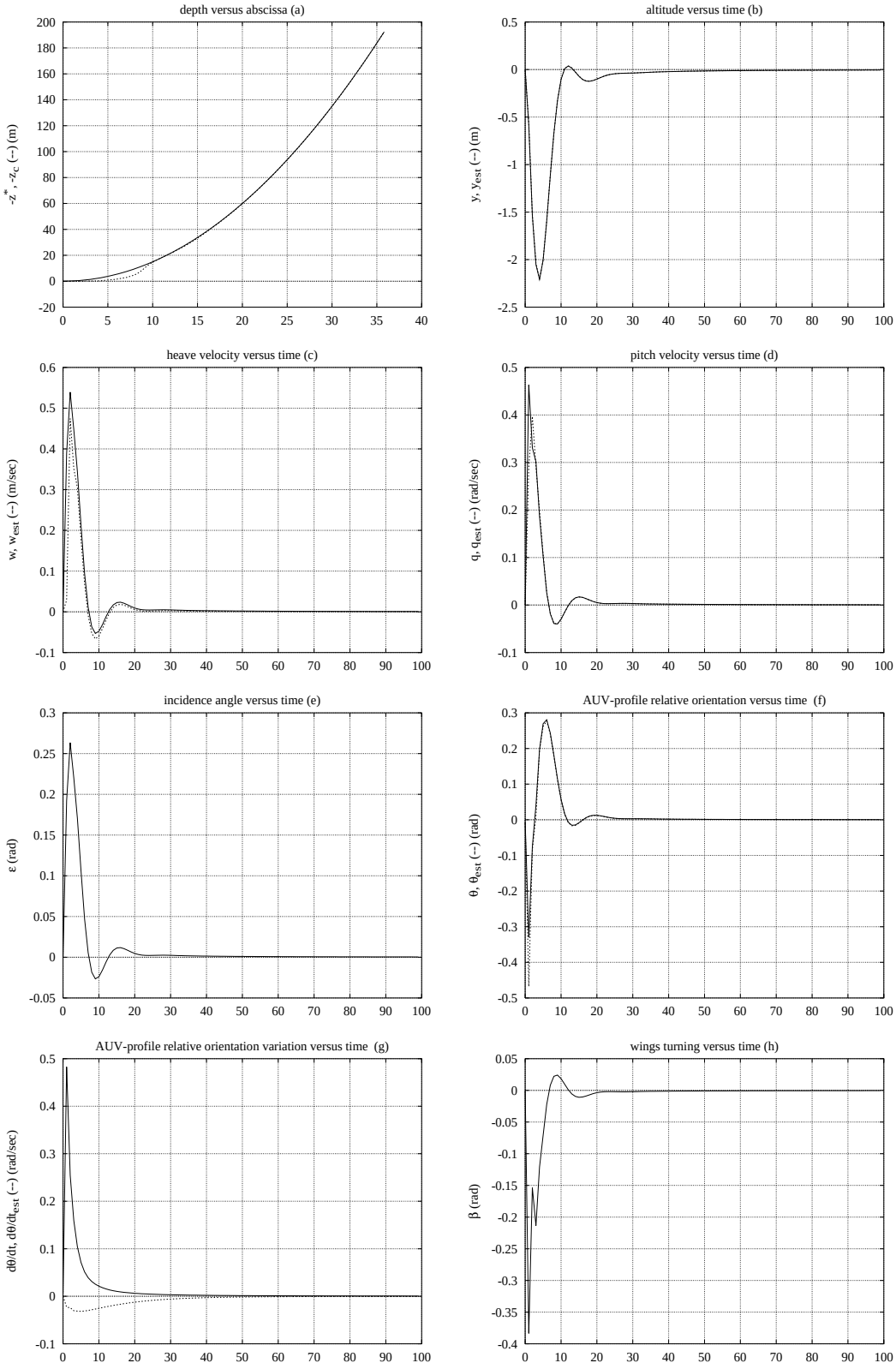

Figure 8: Simulation on parabolic bottom profile using the LQG/LTR+EKF controller. Main parameters value : bottom : $z^* = -0.15x^{*^2} + z0$, vehicle initial orientation=0rad, Rc=30.0, Ro=0.1, Ad=-.1, Cd=-Ad, Gd=5.0 (identical to those for simulations using LQG/LTR controller before)

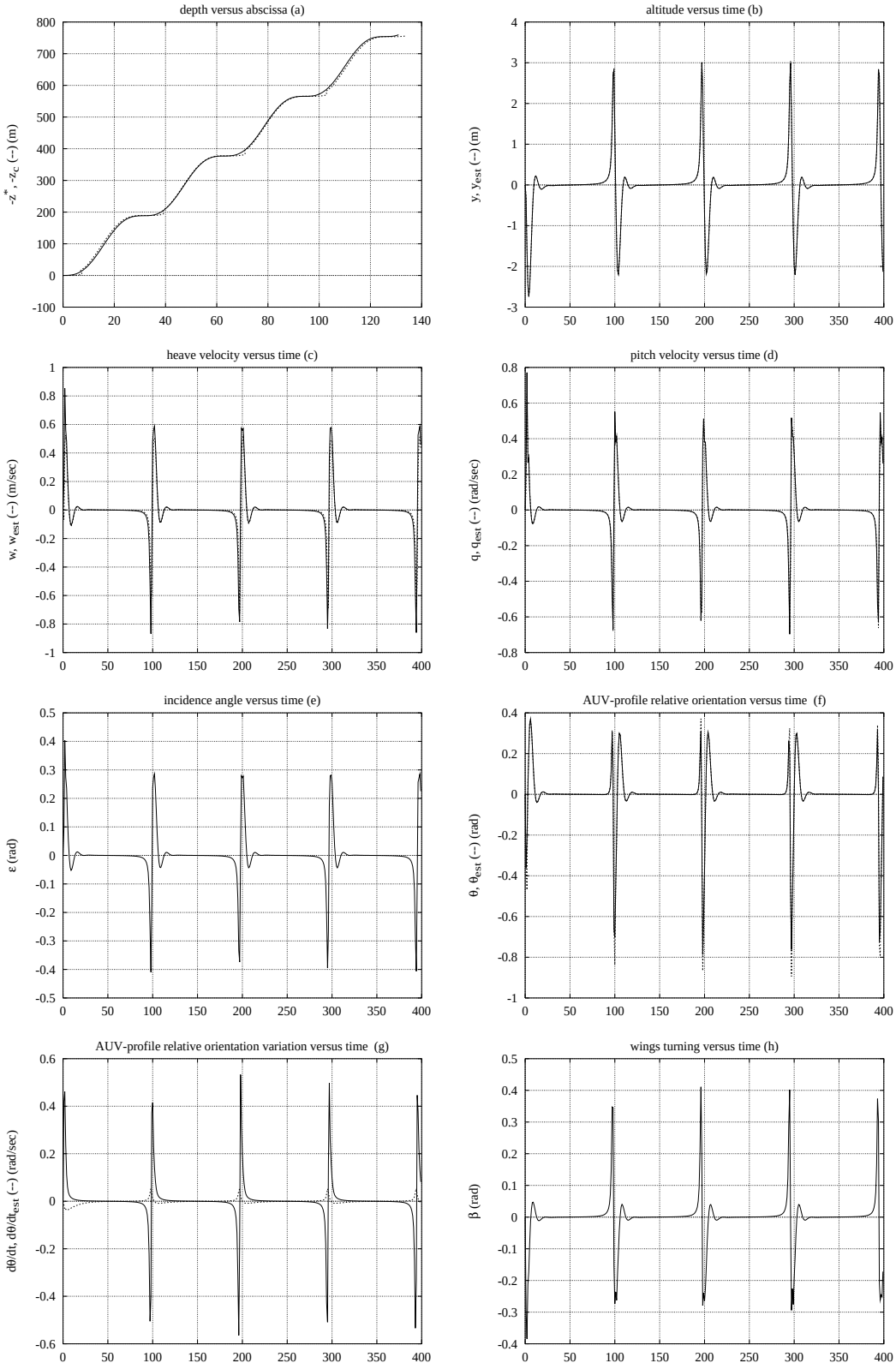

Figure 9: Simulation on "quasi" sinusoidal bottom profile using the LQG/LTR+EKF controller. Main parameters value : bottom period : $\approx 100sec$, vehicle initial orientation=0rad, Rc=30.0, Ro=0.1, Ad=-.1, Cd=-Ad, Gd=5.0 (identical to those for simulations using LQG/LTR controller before)

we are able to access the well-understood design rules for manipulating the performance and robustness of the resulting controller without the need to introduce too many free variables. The final part of our objective is to replicate the nonlinearization of the Kalman filter part by the consideration of nonlinear control computation. As stated at the outset, one reason for selecting LQ controllers was their connection with predictive control methods in the linear case. Accordingly, we seek to generalize the control law by replacing the LQ feedback (20) by a nonlinear predictive controller.

In the recent work of [Michalska and Mayne, 1993], a discrete-time nonlinear predictive control formulation is constructed which possesses several advantageous features :

- It is based on the minimization of a quadratic performance index over a finite horizon into the future. This horizon is a receding horizon, but is not fixed and may change from moment to moment. Indeed, the horizon is part of the optimization itself. Thus at time t we solve :

$$\min_{u \in \mathcal{U}, T} \int_t^{t+T} \left[\mathbf{x}^T(\tau) \boldsymbol{\mathcal{Q}}_c \mathbf{x}(\tau) + \beta^T(\tau) \mathcal{R}_c \beta(\tau) \right] d\tau$$

  subject to terminal and perhaps other constraints.

- The remainder of the feasible trajectory at time t provides a feasible but sub-optimal trajectory from which to commence the optimization at time $t+1$.

- A stability theory exists in which the terminal constraints permit the proof of closed loop stability with this Receding Horizon controller.

- It has connections to a robustness theory based on the degree of stability that is attained. This robustness is measured in terms of the uncertainty of the state update equation but does not include unmodelled dynamics.

- It relies on full state measurements being available for the re-commencement of the controller computation.

From the perspective of the AUV problem, this nonlinear predictive control formulation is pertinent. It suggests that we might replace the LQ component of the linear design by this, and preserve the design aspects and the limiting behaviour for small signals. When combined with the discrete-time results of [LaScala et al., 1995] on the design of the EKF to yield bounded state errors, a fuller robust stability theory begin to emerge. The experimental work remains to be done, however.

7 Conclusion

We have presented an approach to nonlinear control design which preserves contact with the design rules of linear controllers. That is, we emphasize the *design* aspects. The motivating problem is the bottom-following control of an autonomous underwater vehicle, which demonstrates aspects of nonholonomic and nonminimum-phase behaviour and so is not particularly well suited to feedback linearization or inversion solutions. This following task is specified with a single measurement of current altitude alone, i.e. with no look-ahead capability, that has proven to be sufficient for profile curves of class at least $\mathcal{C}^1$. The nonlinear control method is developed by migrating an LQG/LTR controller for the linearized model to include a modified extended Kalman filter. The resulting controller maintains the prospect of alteration of closed loop performance via weighting selection or the introduction of frequency-weighting without compromising design simplicity and understanding.

Simulation studies using fully nonlinear dynamical models of the AUV demonstrate the benefits of the method for this task. A further development avenue is also highlighted which also replaces the linear state feedback by a nonlinear predictive controller. Work is proceeding to evaluate the benefits here.

The work of this paper presents new results in the three areas of :

- generic nonlinear control design as a migration of linear design,
- generic formulation of a control problem of a mechanical device in an unstructured environment as disturbance rejection,
- application of these ideas to the AUV problem.

A AUV characteristics : numerical data used in simulation

```
Cxu = -51.0;            // AUV Hydrodynamics coefficients
Czw = -303.0;
Czq = -300.0;
Cmw = 303;
Cmq = -360.0;
Dh = [ Cxu, 0.0, 0.0 ; 0.0, Czw, Czq ; 0.0, Cmw, Cmq ];

m = 800.0;              // vehicle mass
g = 9.8;                // gravity
xg = 0.0;               // center of gravity coordinates
zg = 0.0;
xf = 0.0;               // buoyancy point coordinates
zf = 0.0;
rho = 1025.0;           // sea-water density
Vol = m/rho;            // for a neutral buoy AUV

Xu_p = 0.0;             // added inertia
Xw_p = 0.0;             // WARNING : ??_p always negative !
Xq_p = 0.0;
Xw_p = 0.0;
Zw_p = 0.0;
Zq_p = 0.0;
Mq_p = 0.0;

Iyy = 660.0;            // inertia around Oy
                        // inertia matrix Mi and its inverse Mi_1
Mi = [  m-Xu_p, -Xw_p, m*zg-Xq_p;
        -Xw_p, m-Zw_p, -m*xg-Zq_p;
        m*zg-Xq_p, -m*xg-Zq_p, Iyy-Mq_p ];
if (det(Mi) <> 0) then,
        Mi_1 = inv(Mi);
else,
        error('*** Error : inertia matrix not inversible ');
end,
                        // Fcoriolis = m*q(t)*Cr*\un{w}(t) <-- Cr
Cr = [ 0.0, -1.0, xg ; 1.0, 0.0, zg ; -xg, -zg, 0.0 ];
                        // actuators (mobile wings) characteristics
Czow = 1.25/(15*(\%pi)/180.0);  // lift reference coefficient
Cxow = 0.01;                    // drag reference coefficient
daw = -1.5;                     // wing loc distance from C (vehicle ref point)
cw = 0.2;                       // wing cord
bw = 1.0;                       // wing span
```

```
Sw = bw*cw;                        // total surface
lefw = 4.0*(bw)/(cw);              // allongement
Betamax = 90.0*(\%pi)/180.0;      // actuator max angle turning
                          // actuators (screw propeller) characteristics
Ct0p = 0.50539; Ct1p = -0.088971; Ct2p = -0.22960; Ct3p = 0.046836;
Cq0p = 0.090271; Cq1p = -0.013470; Cq2p = -0.023529; Cq3p = -0.002005;
Cnp = 0.1;                         // hydro coeffs
Dpo = 0.4;                         // screw diameter
dap = -1.75;              // propeller loc dist from C (vehicle ref pt)
```

B Frequency-weighted LGQ with emphasis on the AUV

Consider the LQG disturbance rejection problem depicted on Figure 10 with criterion function :

$$J = \lim_{N\to\infty} \frac{1}{N} \left(y_i^2 + \lambda u_{\beta_i}^2 \right) \tag{29}$$

where the aim is to minimize J over all internally stabilizing controller C, and where the disturbance d_t is modelled as the output of a linear system H driven by a gaussian white noise e_t of unit variance. P represents the (auv + environment-interaction) process.

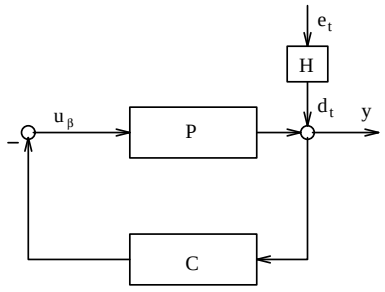

Figure 10: LQG disturbance rejection loop

In this framework, we have :

$$y = \frac{H}{1 + PC_{LQ}} e_t \quad \text{and} \quad u_\beta = \frac{-C_{LQ}}{1 + PC_{LQ}} e_t$$

Using Parseval's formula, the criterion J (29) may be rewritten as :

$$J \;=\; \frac{1}{2\pi} \int_{-\pi}^{+\pi} \frac{1 + \lambda |C_{LQ}|^2}{|1 + PC_{LQ}|^2} |H|^2 dw \;\triangleq\; J_{LQ}(P, H, \lambda) \tag{30}$$

Now consider the same loop but with a frequency-weighted criterion :

$$J_{FW} = \lim_{N\to\infty} \frac{1}{N} \left((F_1 y_i)^2 + \lambda (F_2 u_{\beta_i})^2 \right) \tag{31}$$

where F_1 and F_2 are stable and stably invertible filters expressing a frequency-variation of the cost. Using Parseval's formula again yields :

$$J_{FW} = \frac{1}{2\pi}\int_{-\pi}^{+\pi} \frac{|F_1|^2 + \lambda|F_2|^2|C_{FW}|^2}{|1+PC_{FW}|^2}|H|^2 dw \tag{32}$$

Rearranging terms yields :

$$J_{FW} = \frac{1}{2\pi}\int_{-\pi}^{+\pi} \frac{1+\lambda|F_1^{-1}F_2C_{FW}|^2}{|1+(PF_2^{-1}F_1)(F_1^{-1}F_2C_{FW})|^2}|F_1H|^2 dw \tag{33}$$

Thus the solution C_{FW} of the frequency-weighted problem under criterion (33), and regarding (30), is given by :

$$C_{FW} = F_2^{-1}F_1C_{LQ}(PF_2^{-1}F_1, F_1H, \lambda) \tag{34}$$

For example, with the AUV we only desire to penalize output deviations in the low-frequency range while not permitting too sharp a variation of the command signal. For this case, we may therefore take F_1 as low-pass and F_2 as flat or high-pass dominant. This would yield :

$$\begin{aligned} \bar{P} &= PF_2^{-1}F_1 = P \text{ x } (low-pass) \\ \bar{H} &= HF_1 = H \text{ x } (low-pass) \\ \bar{C} &= C_{LQ}(\bar{P}, \bar{H}, \lambda) \end{aligned}$$

Then the controller to be implemented on P, C_{FW}, is computed as $C_{FW} = F_2^{-1}F_1\bar{C}$ or $\bar{C}$ x $(low-pass)$. In this way, loop-shaping for performance is achieved without loss of closed-loop stability. Figure 11 draws the $\bar{P}$, $\bar{H}$ control loop for the $\bar{C}$ design.

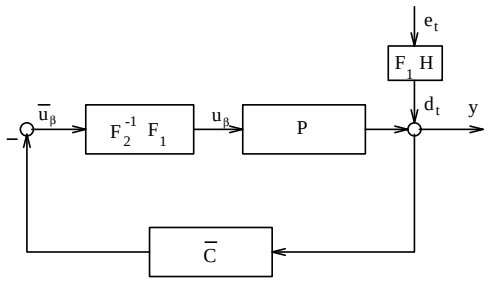

Figure 11: Frequency-weighted LQG disturbance rejection loop

Denote the states of the whole process depicted in Figure 11 as $\bar{x}_t = (x_3, x, x_f, x_1)$ for components $F_3 = F_2^{-1}F_1$, P, H, F_1 respectively. Then the controller $\bar{C}$ will yield feedback control based on state estimates :

$$\bar{u}_\beta = \bar{K}\begin{bmatrix} \hat{x}_3 \\ \hat{x} \\ \hat{x}_f \\ \hat{x}_1 \end{bmatrix} \tag{35}$$

The other part of $\bar{C}$ will consist of a state estimator. Note however that x_3 and x_1 are directly measurable. The gain is computed directly from a regular Algebraic Ricatti Equation (ARE). Denote the four sub-systems as :

$$\begin{array}{ll} F_3 = [A_3, B_3, C_3, D_3]\,, & P = [A_v, B_v, C_v] \\ F_1 = [A_1, B_1, C_1, D_1]\,, & H = [A_f, B_f, C_f] + R_o^{1/2} \text{ (abuse of notation)} \end{array}$$

where R_o denotes the measurement noise variance. This then yields the control design problem as a standard LQ calculation using the following complete process $[\bar{A}, \bar{B}, \bar{C}, \bar{D}]$:

$$\begin{aligned} \dot{\bar{x}} = \begin{bmatrix} \dot{x}_3 \\ \dot{x} \\ \dot{x}_f \\ \dot{x}_1 \end{bmatrix} &= \begin{bmatrix} A_3 & 0 & 0 & 0 \\ B_v C_3 & A_v & 0 & 0 \\ 0 & 0 & A_f & 0 \\ 0 & 0 & B_1 C_f & A_1 \end{bmatrix} \begin{bmatrix} x_3 \\ x \\ x_f \\ x_1 \end{bmatrix} + \begin{bmatrix} B_3 \\ B_v D_3 \\ 0 \\ 0 \end{bmatrix} \bar{u}_\beta + \begin{bmatrix} 0 & 0 \\ 0 & 0 \\ B_f & 0 \\ 0 & B_1 R_o^{1/2} \end{bmatrix} \begin{bmatrix} \zeta_t \\ \nu_t \end{bmatrix} \\ \bar{y} &= \begin{bmatrix} 0 & C_v & D_1 C_f & C_1 \end{bmatrix} \bar{x} + \begin{bmatrix} 0 & D_1 R_o^{1/2} \end{bmatrix} \begin{bmatrix} \zeta_t \\ \nu_t \end{bmatrix} \end{aligned} \tag{36}$$

where ζ_t and ν_t are respectively the perturbation white gaussian noise and the measurement noise.

The LQ problem can then be solved using conventional tools in order to derive $\bar{u}_\beta = \bar{K}\hat{\bar{x}}$ with Kalman observer :

$$\dot{\hat{\bar{x}}} = \bar{A}\hat{\bar{x}} + \bar{M}(\bar{y} - \hat{\bar{y}}) + \bar{B}\bar{u}_\beta$$

To convert now to the FW controller C_{FW} for the original system, we add in the filter $F_2^{-1}F_1$ in series with $\bar{C}$. With existing relations, this can be done through :

$$\begin{aligned} \dot{\hat{\bar{x}}} &= \bar{A}\hat{\bar{x}} + \bar{M}(\bar{y} - \hat{\bar{y}}) + \bar{B}\bar{u}_\beta \\ \dot{\tilde{x}}_3 &= A_3\tilde{x}_3 + B_3\bar{u}_\beta \\ u_\beta &= C_3\tilde{x}_3 + D_3\bar{u}_\beta \end{aligned} \tag{37}$$

The frequency-weighted controller then has the form :

$$\begin{aligned} \begin{bmatrix} \dot{\hat{x}}_3 \\ \dot{\hat{x}} \\ \dot{\hat{x}}_f \\ \dot{\hat{x}}_1 \\ \dot{\tilde{x}}_3 \end{bmatrix} &= \begin{bmatrix} A_3 & 0 & 0 & 0 & 0 \\ B_v C_3 & A_v & 0 & 0 & 0 \\ 0 & 0 & A_f & 0 & 0 \\ 0 & 0 & B_1 C_f & A_1 & 0 \\ B_3\bar{K}^1 & B_3\bar{K}^2 & B_3\bar{K}^3 & B_3\bar{K}^4 & A_3 \end{bmatrix} \begin{bmatrix} \hat{x}_3 \\ \hat{x} \\ \hat{x}_f \\ \hat{x}_1 \\ \tilde{x}_3 \end{bmatrix} \\ &+ \begin{bmatrix} B_3 \\ B_v D_3 \\ 0 \\ 0 \\ 0 \end{bmatrix} \begin{bmatrix} \bar{K}^1 & \bar{K}^2 & \bar{K}^3 & \bar{K}^4 & 0 \end{bmatrix} \begin{bmatrix} \hat{x}_3 \\ \hat{x} \\ \hat{x}_f \\ \hat{x}_1 \\ \tilde{x}_3 \end{bmatrix} + \begin{bmatrix} \bar{M}^1 \\ \bar{M}^2 \\ \bar{M}^3 \\ \bar{M}^4 \\ 0 \end{bmatrix} (\bar{y} - \hat{\bar{y}}) \end{aligned}$$

$$u_\beta = \left[\begin{array}{ccccc} D_3\bar{K}^1 & D_3\bar{K}^2 & D_3\bar{K}^3 & D_3\bar{K}^4 & C_3 \end{array} \right] \left[\begin{array}{c} \hat{x}_3 \\ \hat{x} \\ \hat{x}_f \\ \hat{x}_1 \\ \tilde{x}_3 \end{array} \right] \tag{38}$$

Now we note that the controller $\bar{C}$ is based on the Kalman filter of Figure 11. Here the first filter, F_3 with state x_3, is fully known (including initial state) together with its driving signal $\bar{u}_\beta$. Further, by construction, we know that A_3 is stable. Therefore $\bar{M}^1 = 0$ and the estimator proceeds by simulation without output injection for this component.

Further if we consider state $\tilde{x}_3$ for which we also are able to specify the initial state, we have :

$$\dot{\hat{x}}_3 - \dot{\tilde{x}}_3 = A_3\hat{x}_3 + B_3\bar{K}\bar{x} - B_3\bar{K}\bar{x} - A_3\tilde{x}_3 = A_3(\hat{x}_3 - \tilde{x}_3)$$

Accordingly, if $\hat{x}_3(t = 0) = \tilde{x}_3(t = 0)$, we have for each time instant t : $\hat{x}_3(t) = \tilde{x}_3(t)$.

Next we note that with this observation, the $\hat{x}$ differential equation may be rewritten :

$$\dot{\hat{x}} = A_v\hat{x} + B_v u_\beta$$

Finally we note from the structure (37) that the signals u_β, $\bar{y}$ and $\hat{\bar{y}}$ are preserved outside the linear control calculation. Thus, should there be explicit known process nonlinearities at the control entry or at the output, there may be accommodated in the design while maintaining the FWLQG-based gain calculation.

C More simulation results

C.1 $u_0 = 1m/sec$

Figures 12–17 give some results obtained at an axial nominal advancement velocity $u_0 = 1m/sec$ when following three types of bottom profiles : inclined linear curve, parabolic curve and a "quasi" sinusoidal one. Tests have been conducted with both linear LQG/LTR and LQG/LTR+EKF controllers.

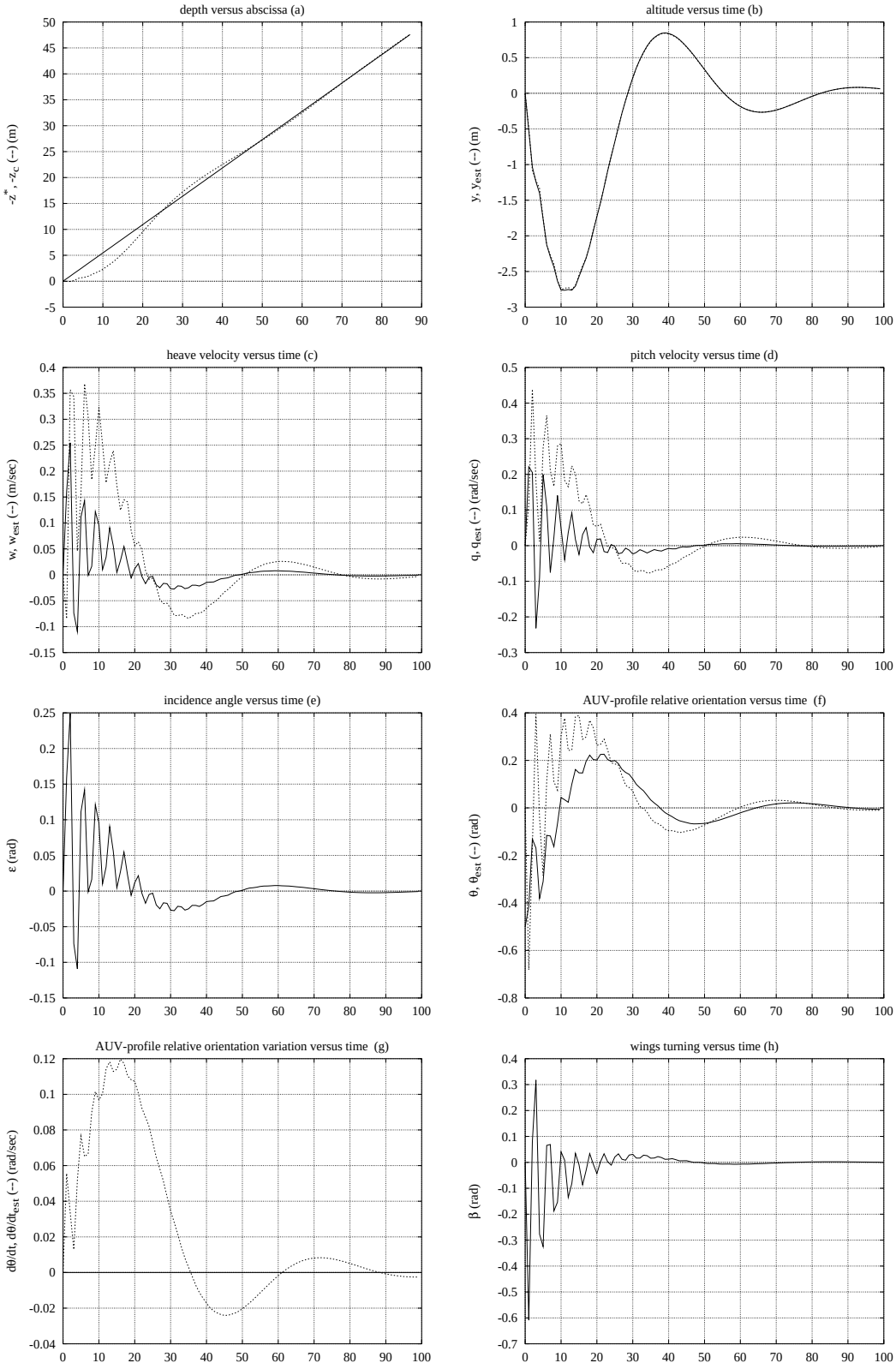

Figure 12: Simulation on linear bottom profile using the LQG/LTR linear controller. Main parameters value : bottom slope=0.5rad, vehicle initial orientation=0rad, Rc=30.0, Ro=0.1, Ad=-.1, Cd=-Ad, Gd=5.0. Advancement velocity : $u_0 = 1m/sec$

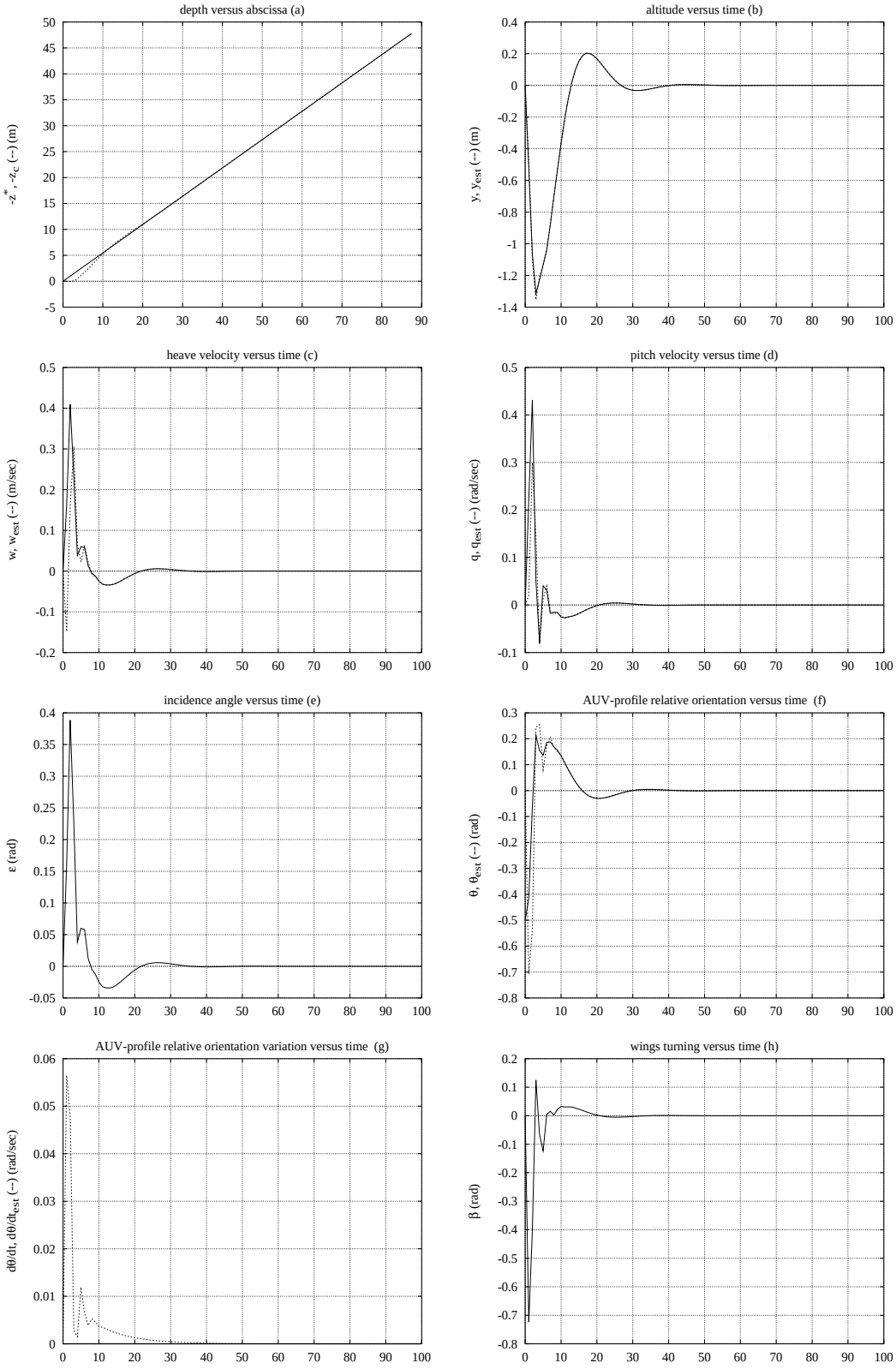

Figure 13: Simulation on linear bottom profile using the LQG/LTR+EKF controller. Main parameters value : bottom slope=0.5rad, vehicle initial orientation=0rad, Rc=30.0, Ro=0.1, Ad=-.1, Cd=-Ad, Gd=5.0. Advancement velocity : $u_0 = 1m/sec$

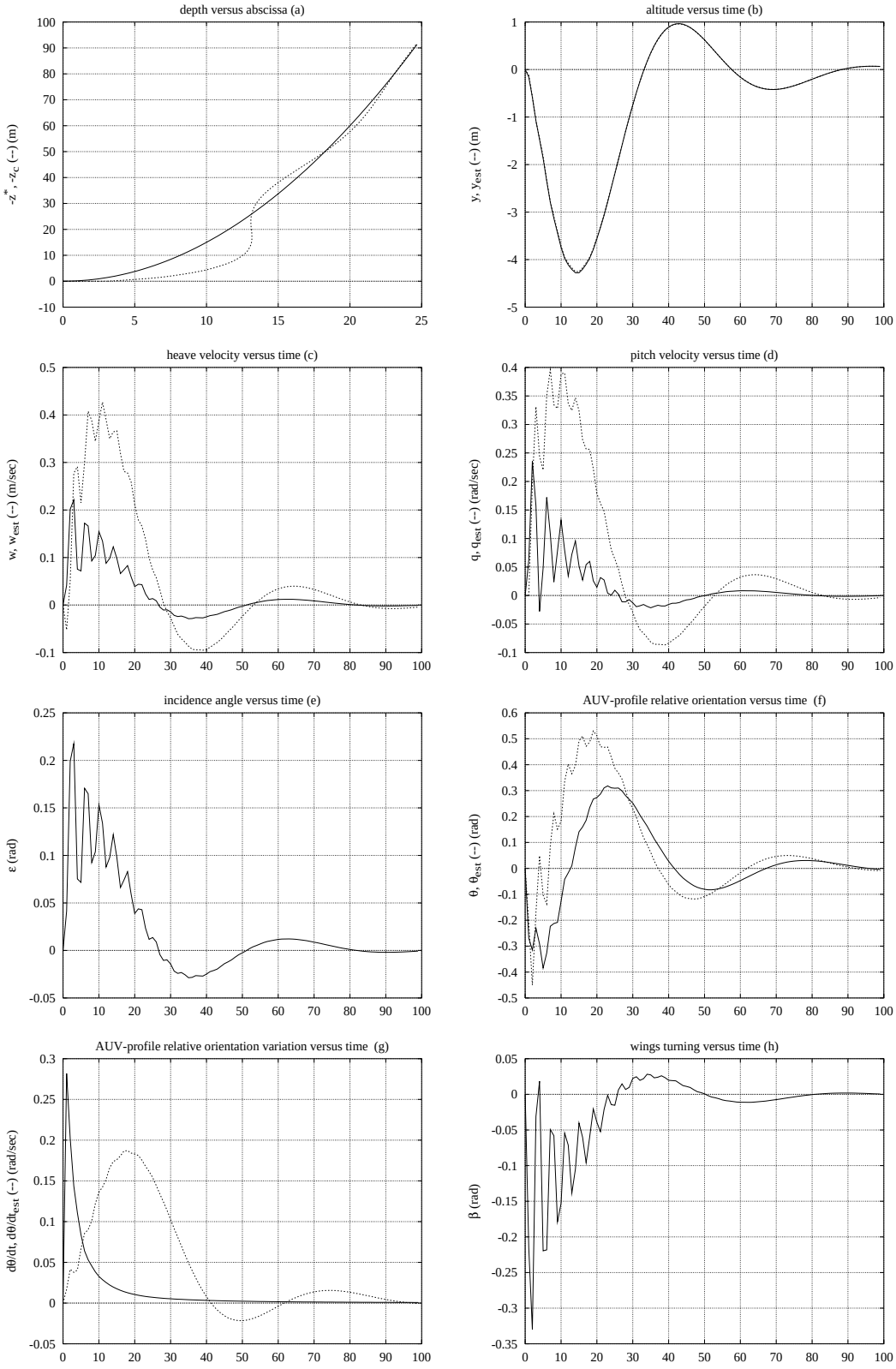

Figure 14: Simulation on parabolic bottom profile using the LQG/LTR controller. Main parameters value : bottom : $z^* = -0.15x^{*^2} + z0$, vehicle initial orientation=0rad, Rc=30.0, Ro=0.1, Ad=-.1, Cd=-Ad, Gd=5.0. Advancement velocity : $u_0 = 1m/sec$

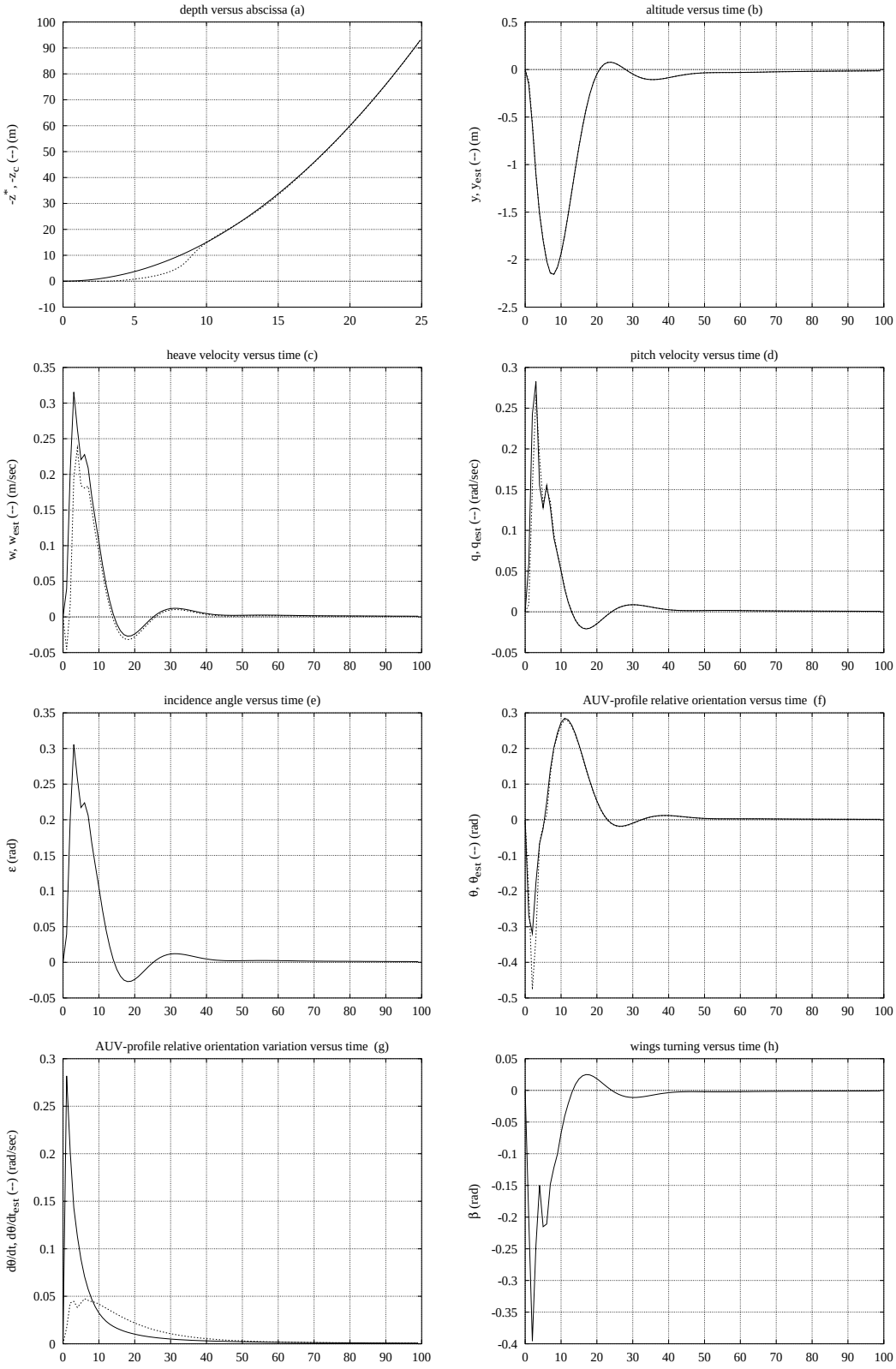

Figure 15: Simulation on parabolic bottom profile using the LQG/LTR+EKF controller. Main parameters value : bottom : $z^* = -0.15x^{*^2} + z0$, vehicle initial orientation=0rad, Rc=30.0, Ro=0.1, Ad=-.1, Cd=-Ad, Gd=5.0. Advancement velocity : $u_0 = 1m/sec$

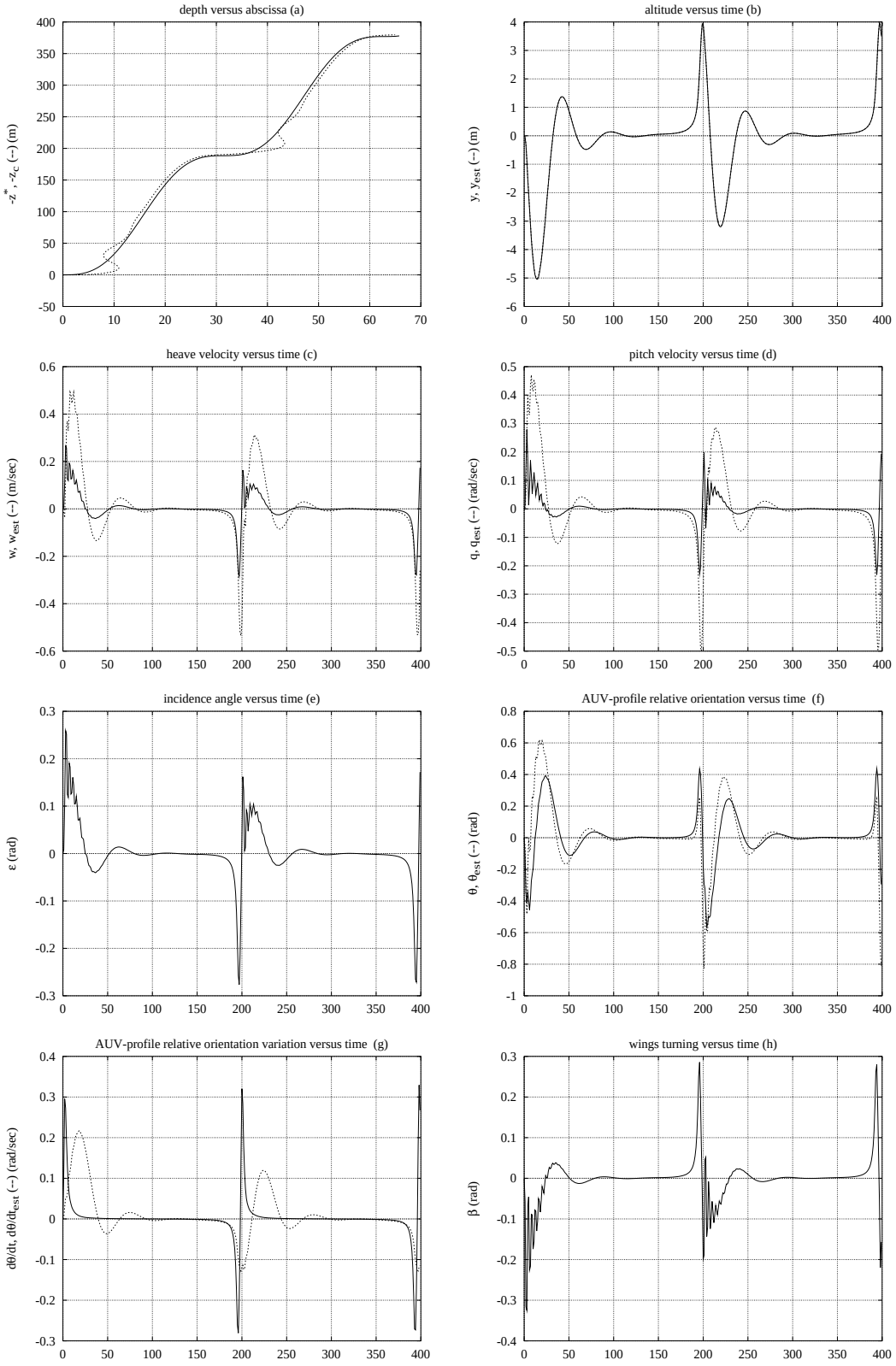

Figure 16: Simulation on "quasi" sinusoidal bottom profile using the LQG/LTR controller. Main parameters value : bottom period : $\approx 210sec$, vehicle initial orientation=0rad, Rc=30.0, Ro=0.1, Ad=-.1, Cd=-Ad, Gd=5.0. Advancement velocity : $u_0 = 1m/sec$

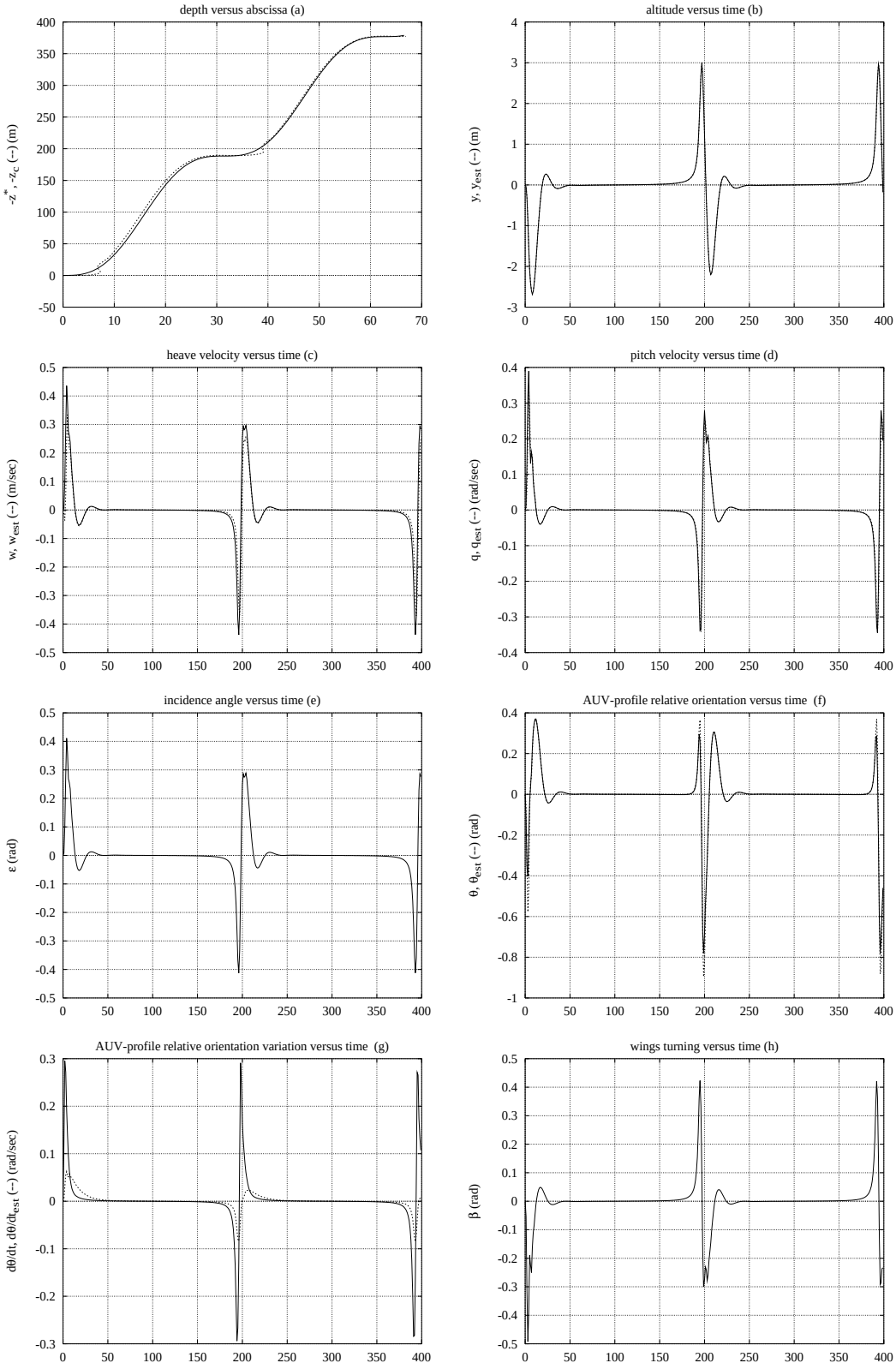

Figure 17: Simulation on "quasi" sinusoidal bottom profile using the LQG/LTR+EKF controller. Main parameters value : bottom period : $\approx 210sec$, vehicle initial orientation=0rad, Rc=30.0, Ro=0.1, Ad=-.1, Cd=-Ad, Gd=5.0. Advancement velocity : $u_0 = 1m/sec$

C.2 $u_0 = 3m/sec$

Figures 18–23 give some results obtained at an axial nominal advancement velocity $u_0 = 3m/sec$ when following three types of bottom profiles : inclined linear curve, parabolic curve and a "quasi" sinusoidal one. Tests have been conducted with both linear LQG/LTR and LQG/LTR+EKF controllers.

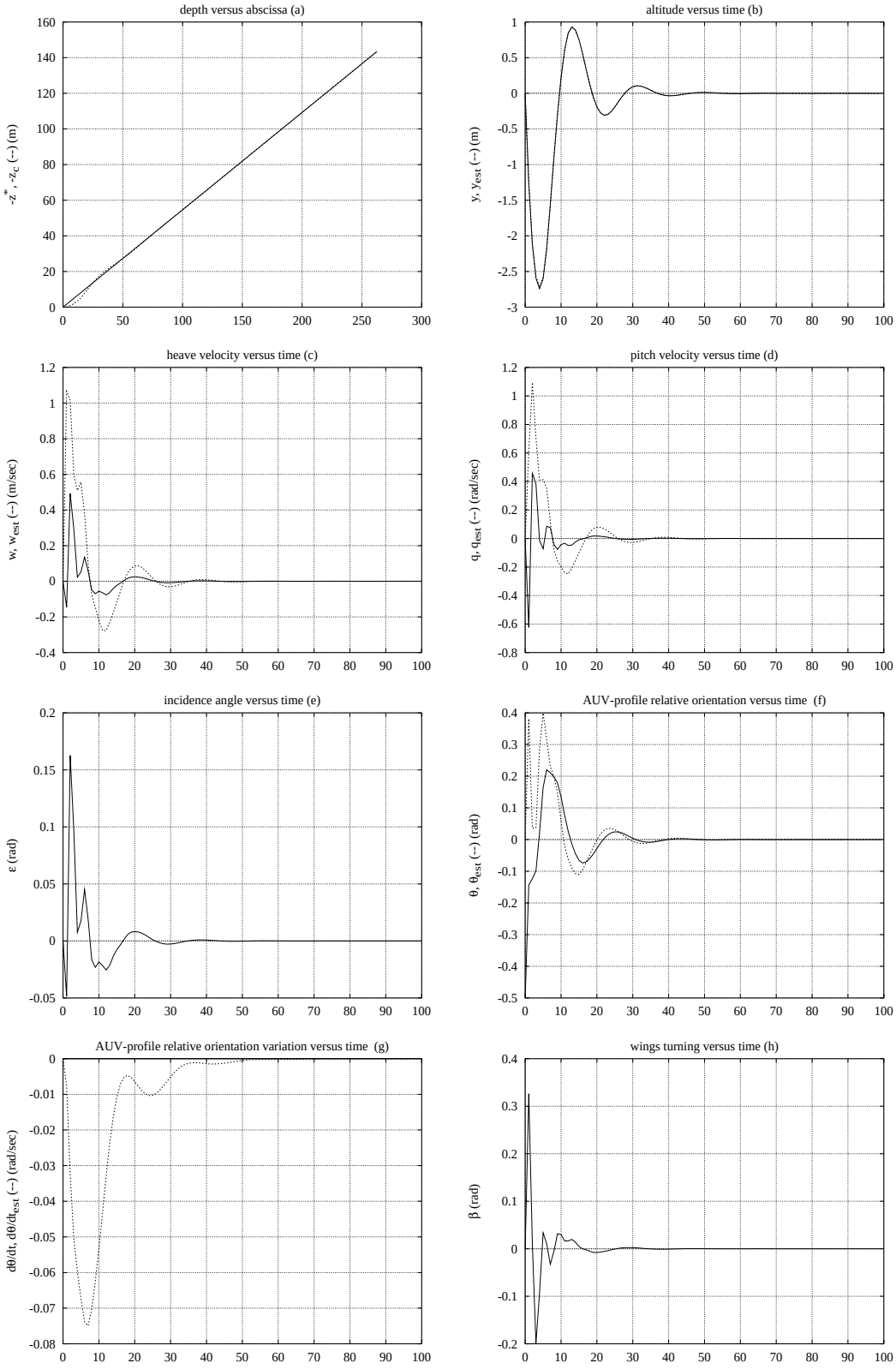

Figure 18: Simulation on linear bottom profile using the LQG/LTR linear controller. Main parameters value : bottom slope=0.5rad, vehicle initial orientation=0rad, Rc=30.0, Ro=0.1, Ad=-.1, Cd=-Ad, Gd=5.0. Advancement velocity : $u_0 = 3m/sec$

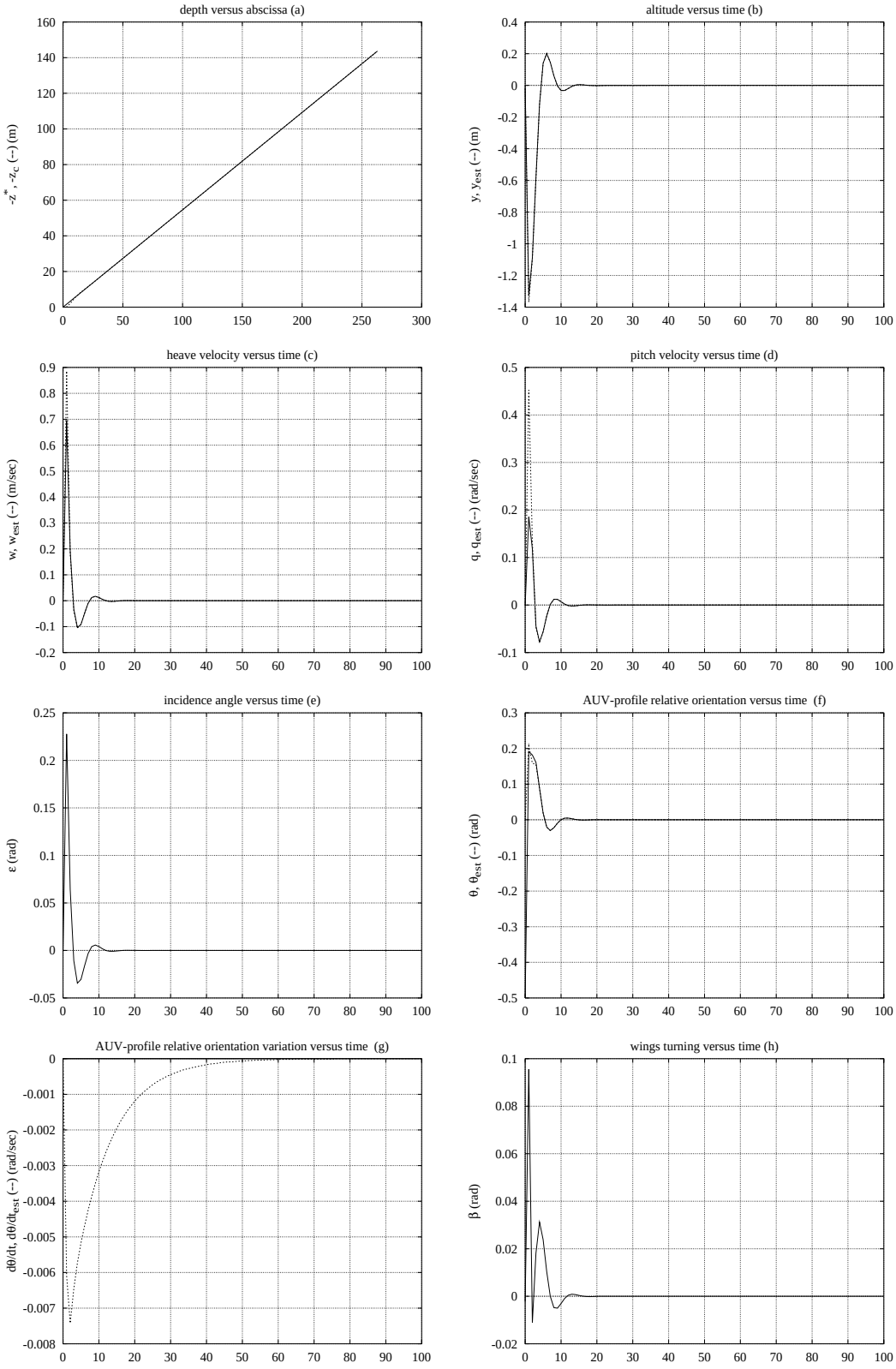

Figure 19: Simulation on linear bottom profile using the LQG/LTR+EKF controller. Main parameters value : bottom slope=0.5rad, vehicle initial orientation=0rad, Rc=30.0, Ro=0.1, Ad=-.1, Cd=-Ad, Gd=5.0. Advancement velocity : $u_0 = 3m/sec$

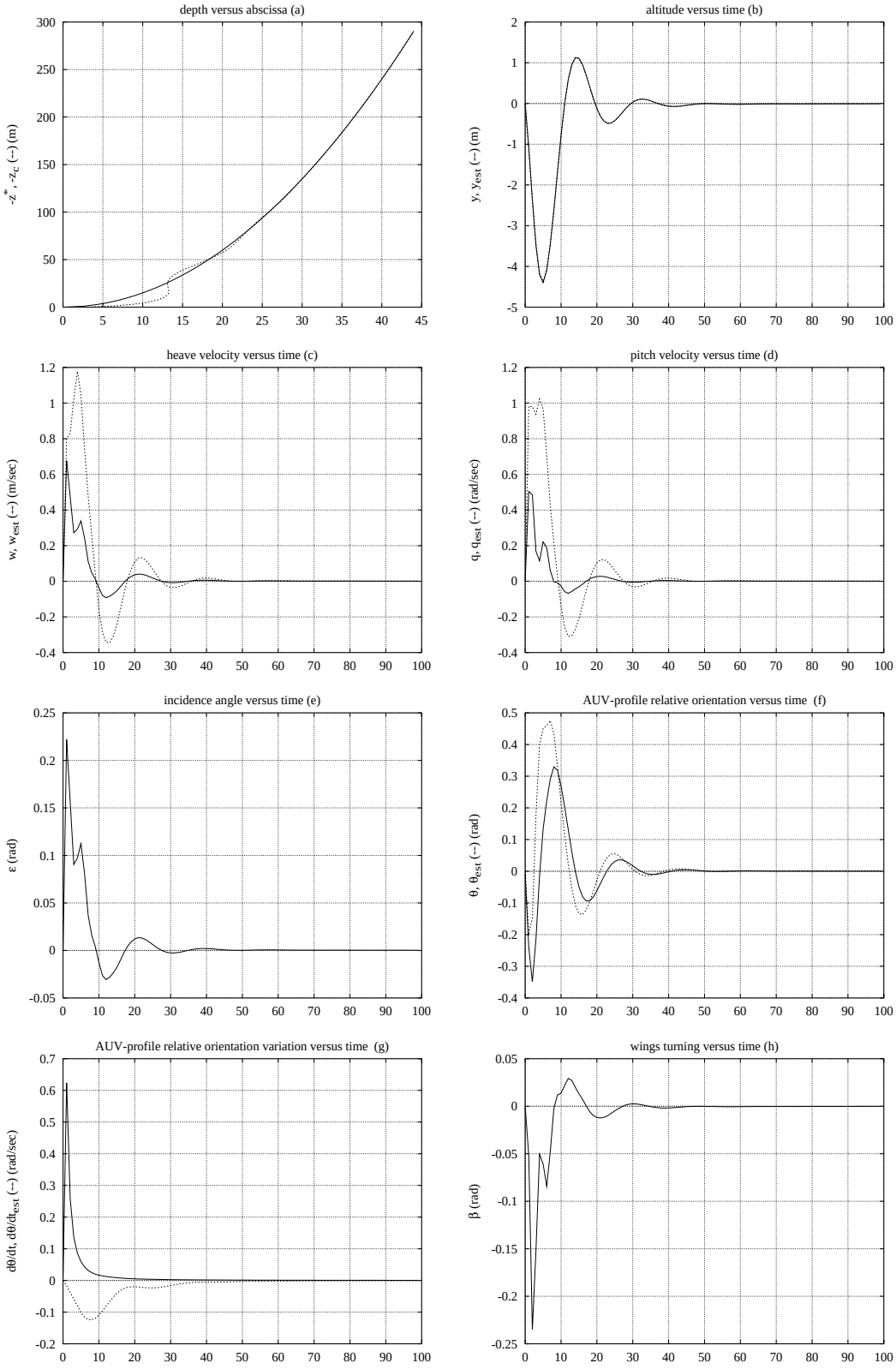

Figure 20: Simulation on parabolic bottom profile using the LQG/LTR controller. Main parameters value : bottom : $z^* = -0.15x^{*^2} + z0$, vehicle initial orientation=0rad, Rc=30.0, Ro=0.1, Ad=-.1, Cd=-Ad, Gd=5.0. Advancement velocity : $u_0 = 3m/sec$

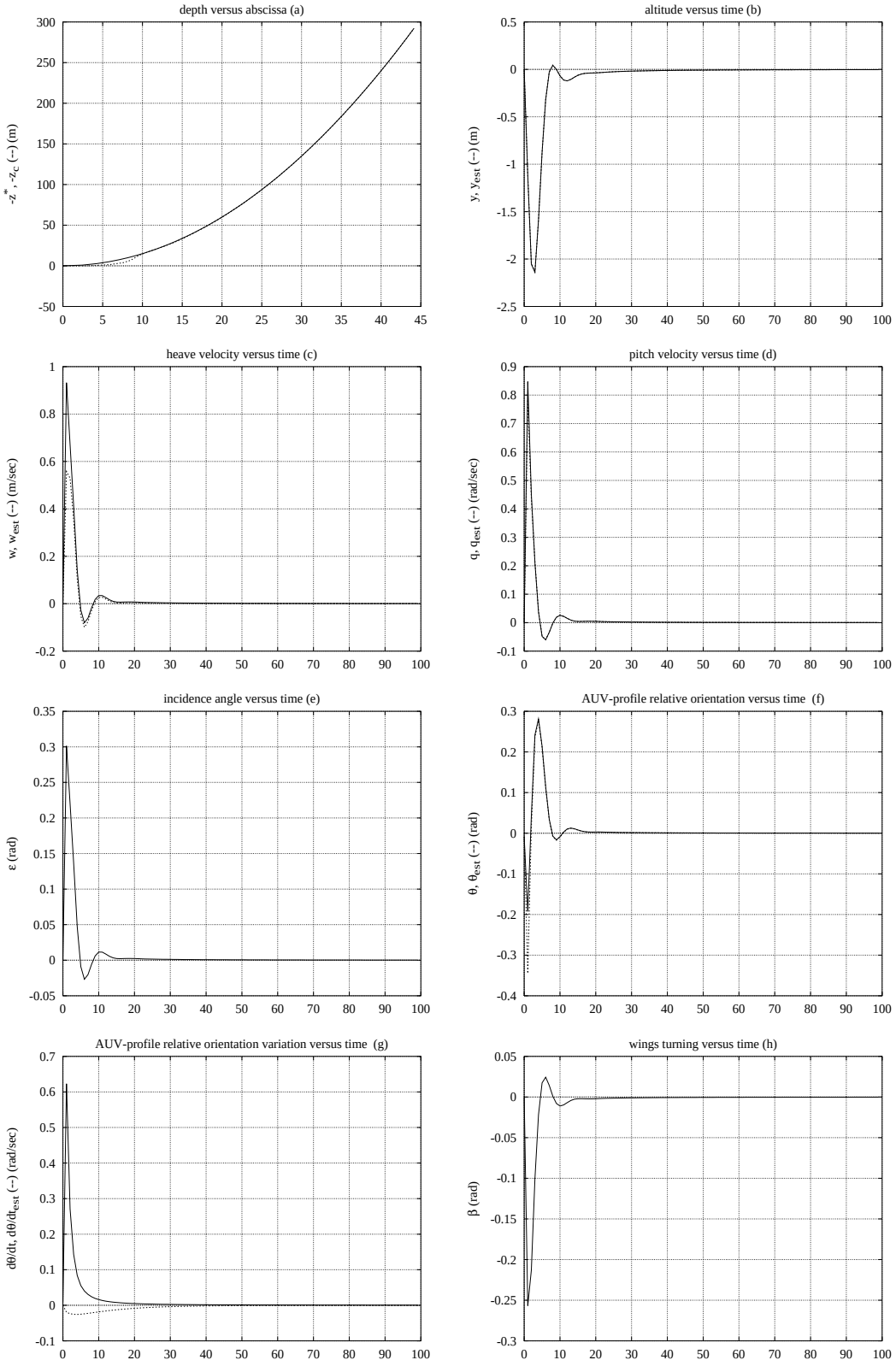

Figure 21: Simulation on parabolic bottom profile using the LQG/LTR+EKF controller. Main parameters value : bottom : $z^* = -0.15x^{*^2} + z0$, vehicle initial orientation=0rad, Rc=30.0, Ro=0.1, Ad=-.1, Cd=-Ad, Gd=5.0. Advancement velocity : $u_0 = 3m/sec$

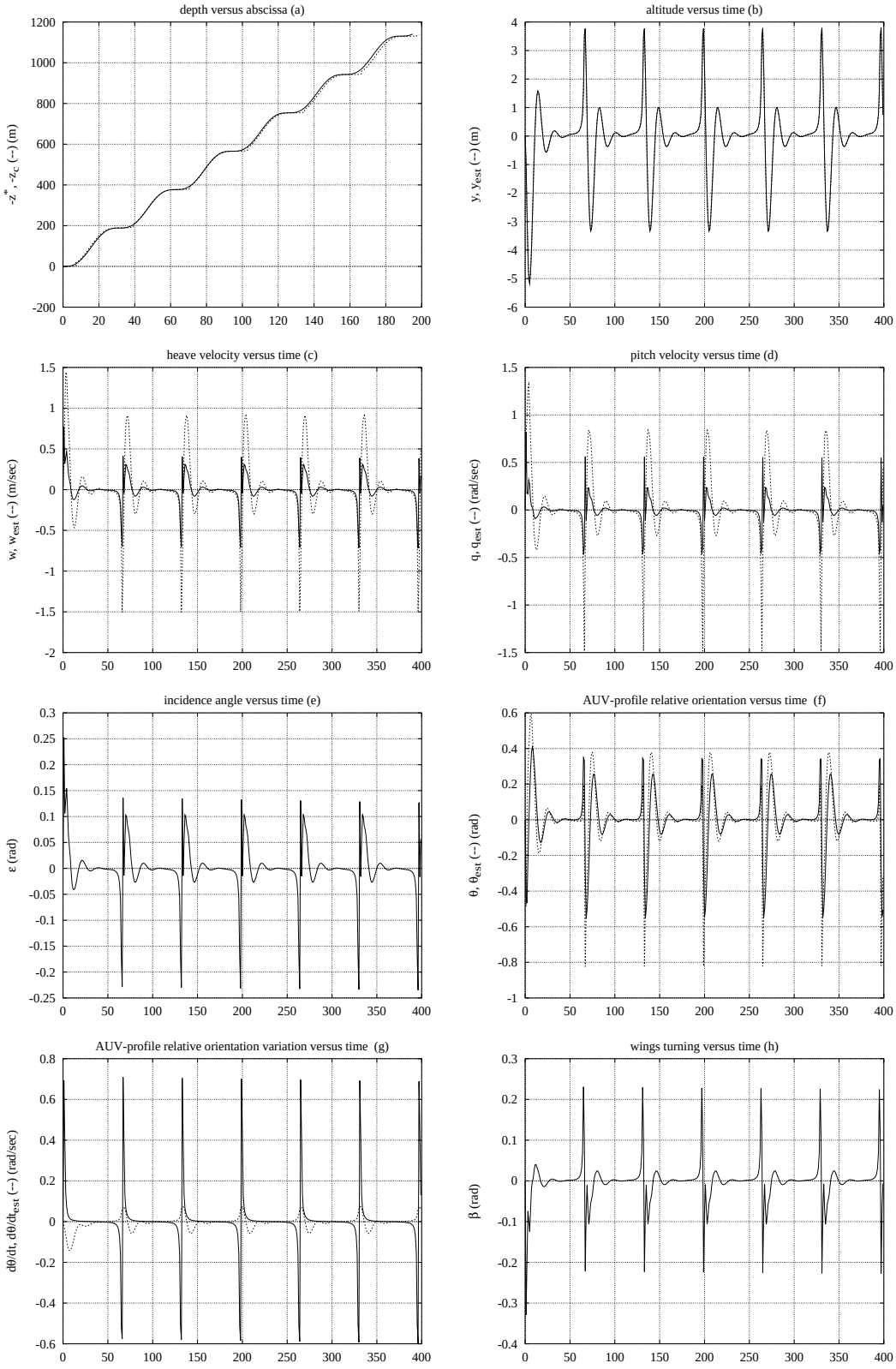

Figure 22: Simulation on "quasi" sinusoidal bottom profile using the LQG/LTR controller. Main parameters value : bottom period : $\approx 70sec$, vehicle initial orientation=0rad, Rc=30.0, Ro=0.1, Ad=-.1, Cd=-Ad, Gd=5.0. Advancement velocity : $u_0 = 3m/sec$

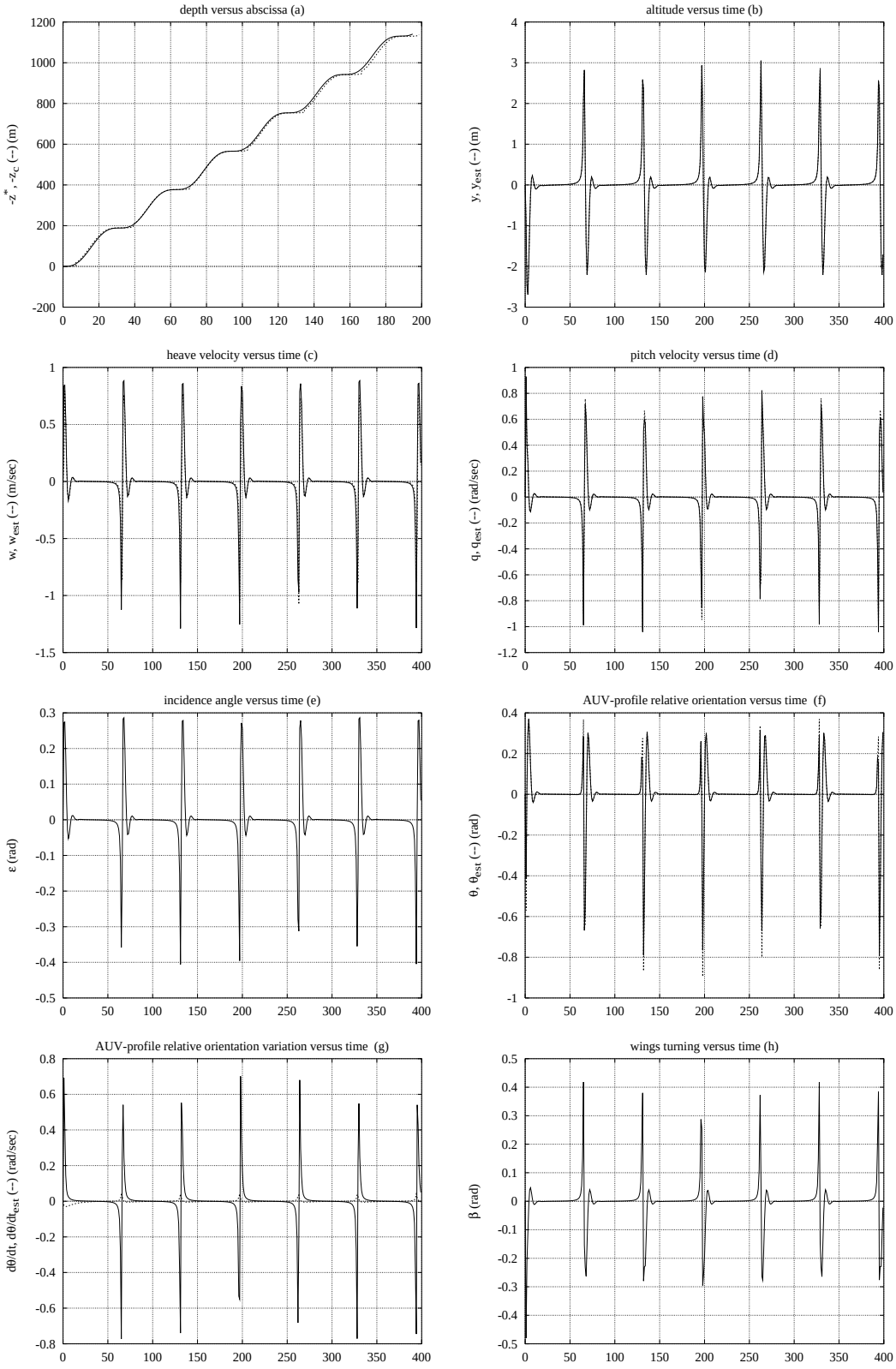

Figure 23: Simulation on "quasi" sinusoidal bottom profile using the LQG/LTR+EKF controller. Main parameters value : bottom period : $\approx 70sec$, vehicle initial orientation=0rad, Rc=30.0, Ro=0.1, Ad=-.1, Cd=-Ad, Gd=5.0. Advancement velocity : $u_0 = 3m/sec$

C.3 Saturation on wings turning : $\beta_M = 10deg$

Figures 24–27 give some results with limited wings turning up to $10deg$, obtained at an axial nominal advancement velocity $u_0 = 2m/sec$ when following two types of bottom profiles : inclined linear curve and parabolic curve. Tests have been conducted with both linear LQG/LTR and LQG/LTR+EKF controllers.

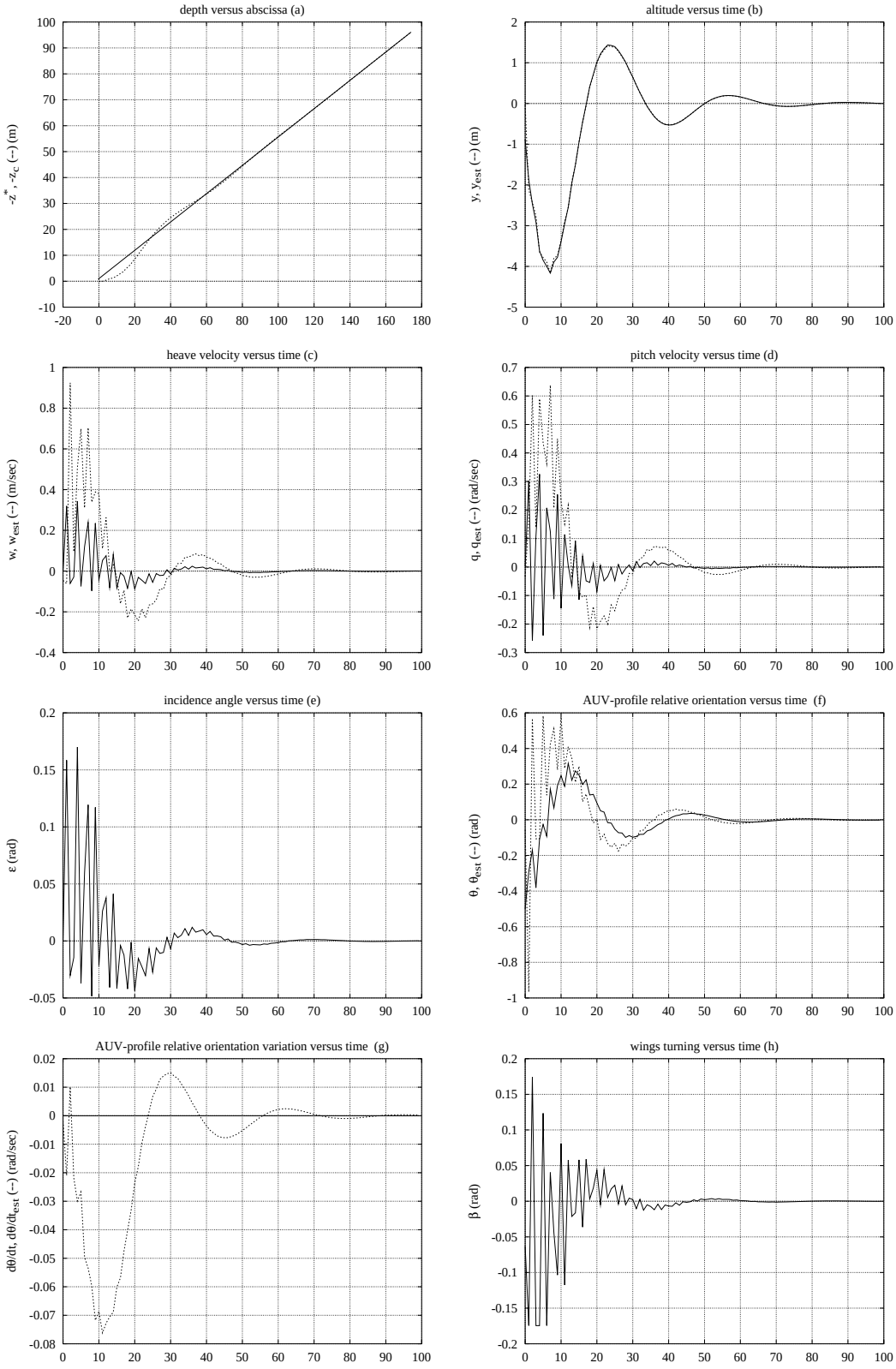

Figure 24: Simulation on linear bottom profile using the LQG/LTR linear controller. Main parameters value : bottom slope=0.5rad, vehicle initial orientation=0rad, Rc=50.0, Ro=1.0, Ad=-.1, Cd=-Ad, Gd=5.0. Advancement velocity : $u_0 = 2m/sec$

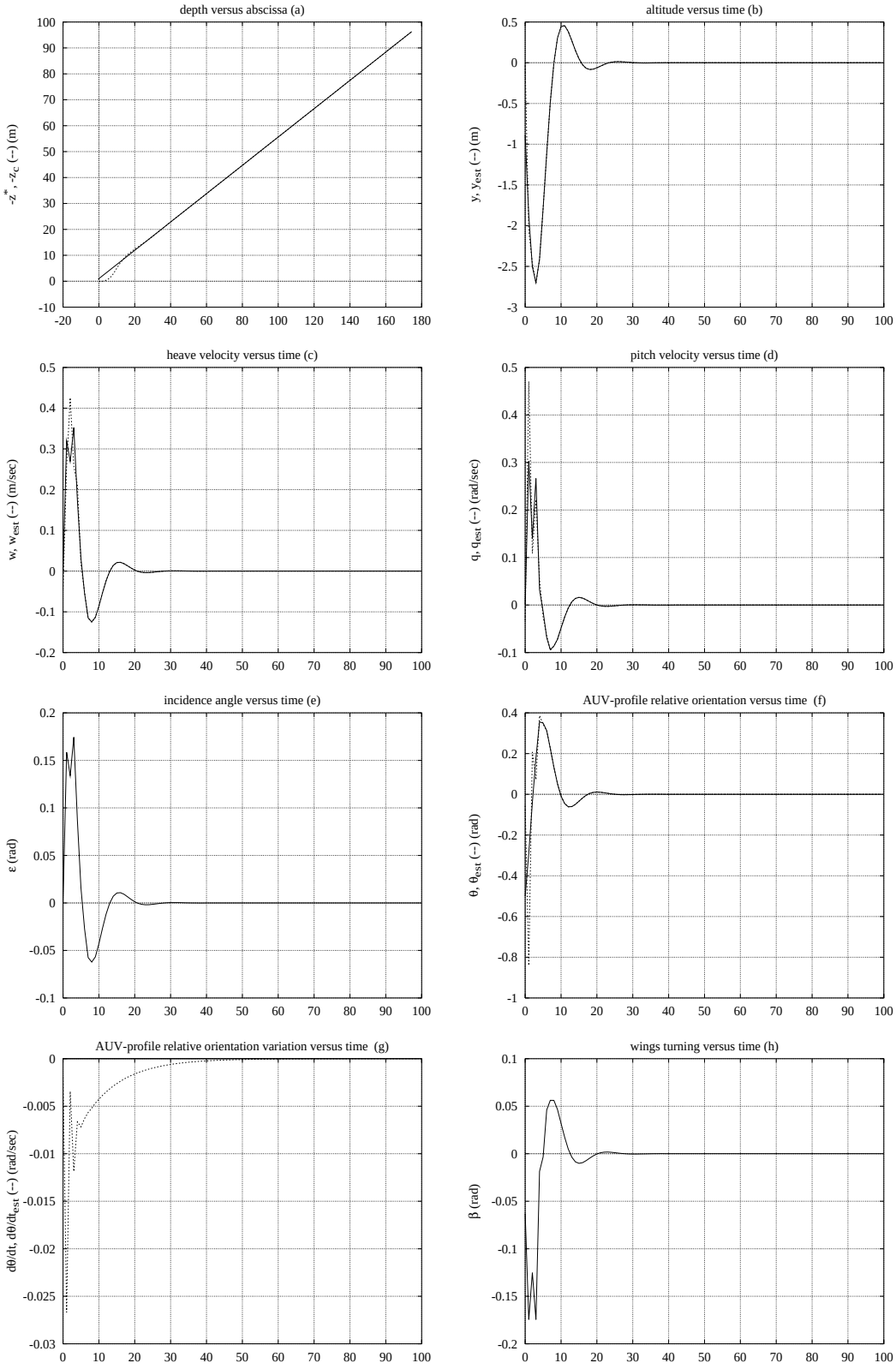

Figure 25: Simulation on linear bottom profile using the LQG/LTR+EKF controller. Main parameters value : bottom slope=0.5rad, vehicle initial orientation=0rad, Rc=50.0, Ro=1.0, Ad=-.1, Cd=-Ad, Gd=5.0. Advancement velocity : $u_0 = 2m/sec$

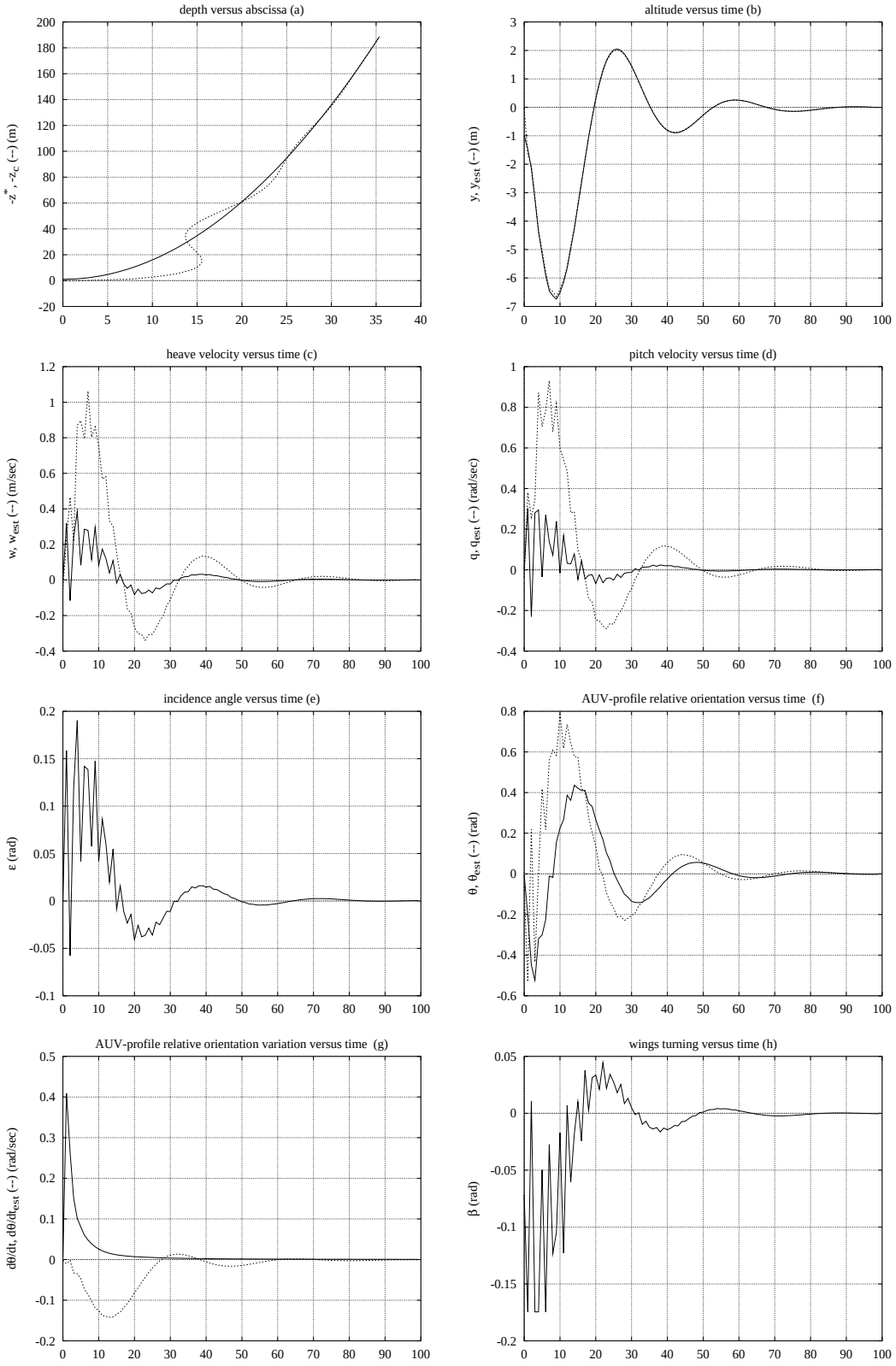

Figure 26: Simulation on parabolic bottom profile using the LQG/LTR controller. Main parameters value : bottom : $z^* = -0.15x^{*^2} + z0$, vehicle initial orientation=0rad, Rc=50.0, Ro=1.0, Ad=-.1, Cd=-Ad, Gd=5.0. Advancement velocity : $u_0 = 2m/sec$

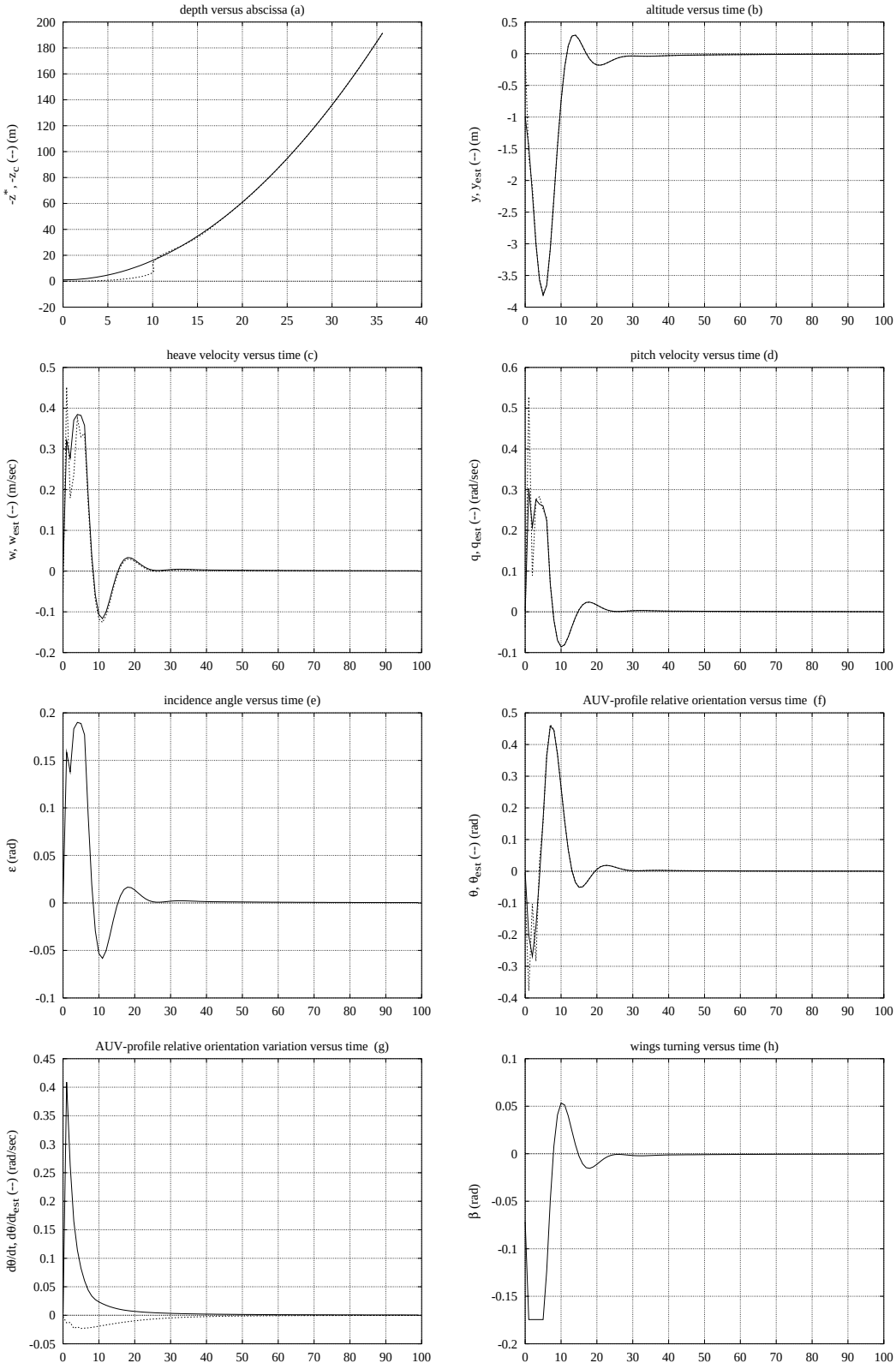

Figure 27: Simulation on parabolic bottom profile using the LQG/LTR+EKF controller. Main parameters value : bottom : $z^* = -0.15x^{*^2} + z0$, vehicle initial orientation=0rad, Rc=50.0, Ro=1.0, Ad=-.1, Cd=-Ad, Gd=5.0. Advancement velocity : $u_0 = 2m/sec$

C.4 Playing with initial conditions : $y(0) = -1m$

Figures 28–31 give some results with $y(0) = 1m$, obtained at an axial nominal advancement velocity $u_0 = 2m/sec$ when following two types of bottom profiles : inclined linear curve and parabolic curve. Tests have been conducted with both linear LQG/LTR and LQG/LTR+EKF controllers.

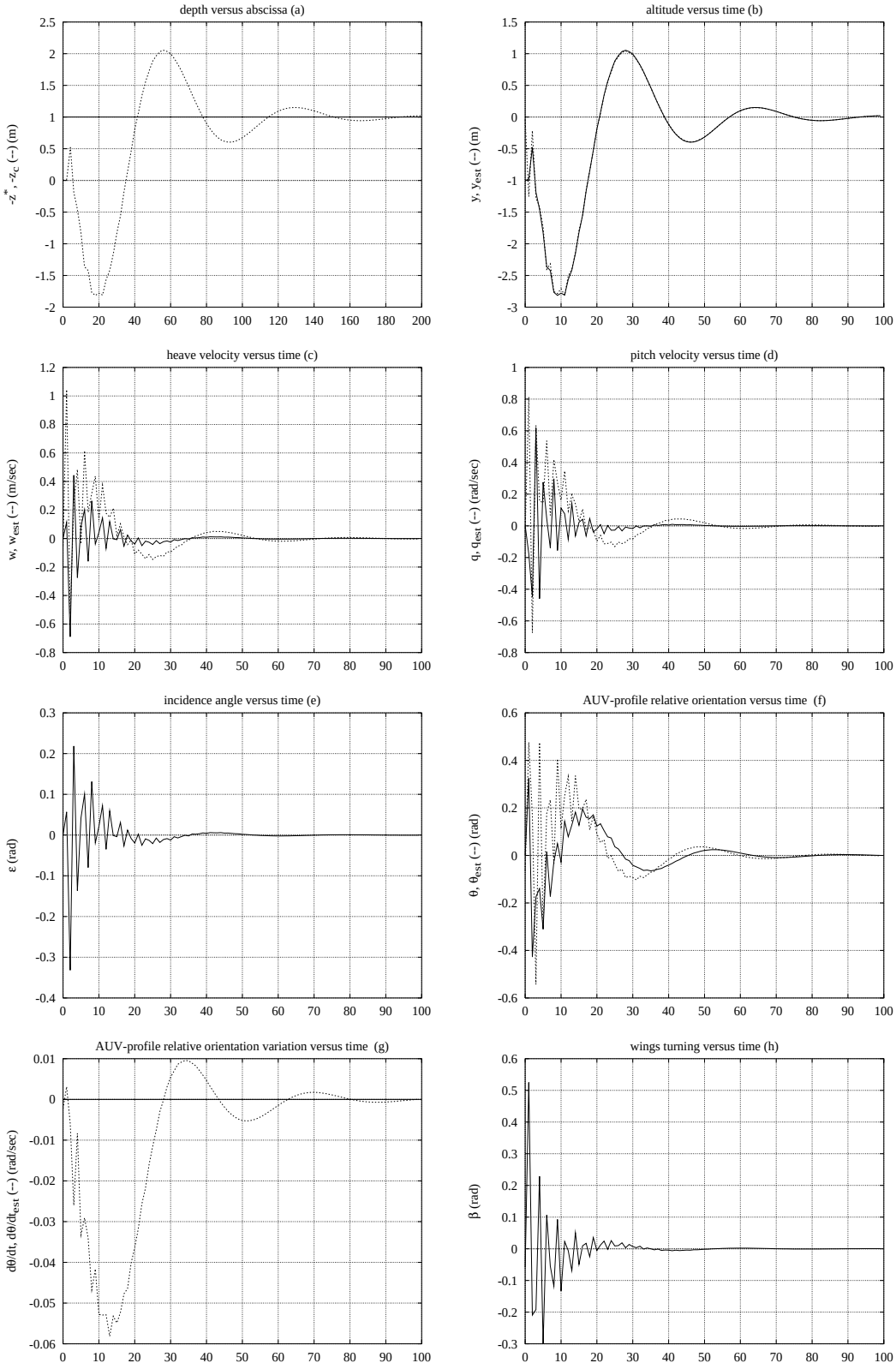

Figure 28: Simulation on linear bottom profile using the LQG/LTR linear controller. Main parameters value : bottom slope=0.5rad, vehicle initial orientation=0rad, Rc=100.0, Ro=1.0, Ad=-.1, Cd=-Ad, Gd=5.0. Advancement velocity : $u_0 = 2m/sec$

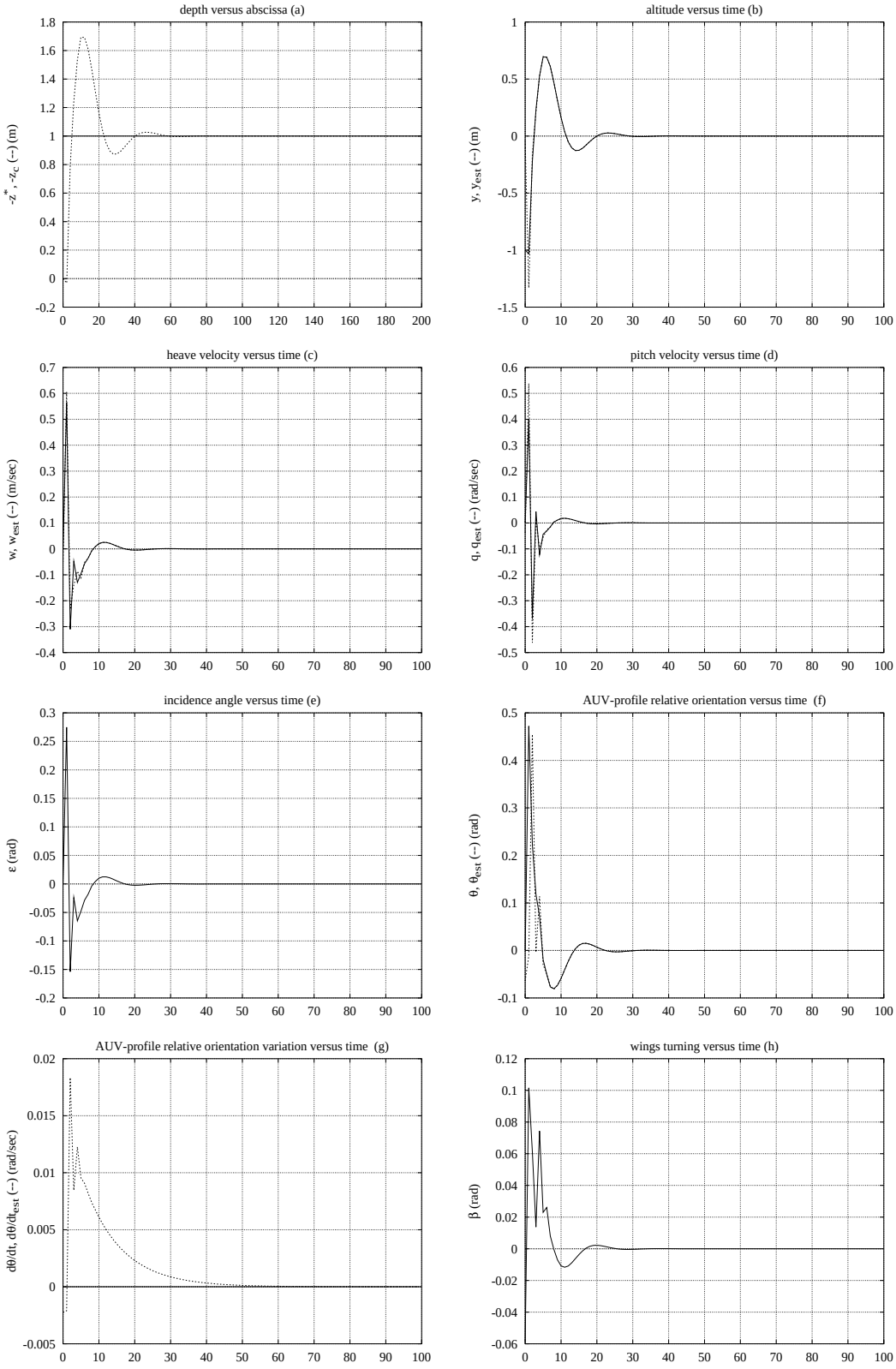

Figure 29: Simulation on linear bottom profile using the LQG/LTR+EKF controller. Main parameters value : bottom slope=0.5rad, vehicle initial orientation=0rad, Rc=100.0, Ro=1.0, Ad=-.1, Cd=-Ad, Gd=5.0. Advancement velocity : $u_0 = 2m/sec$

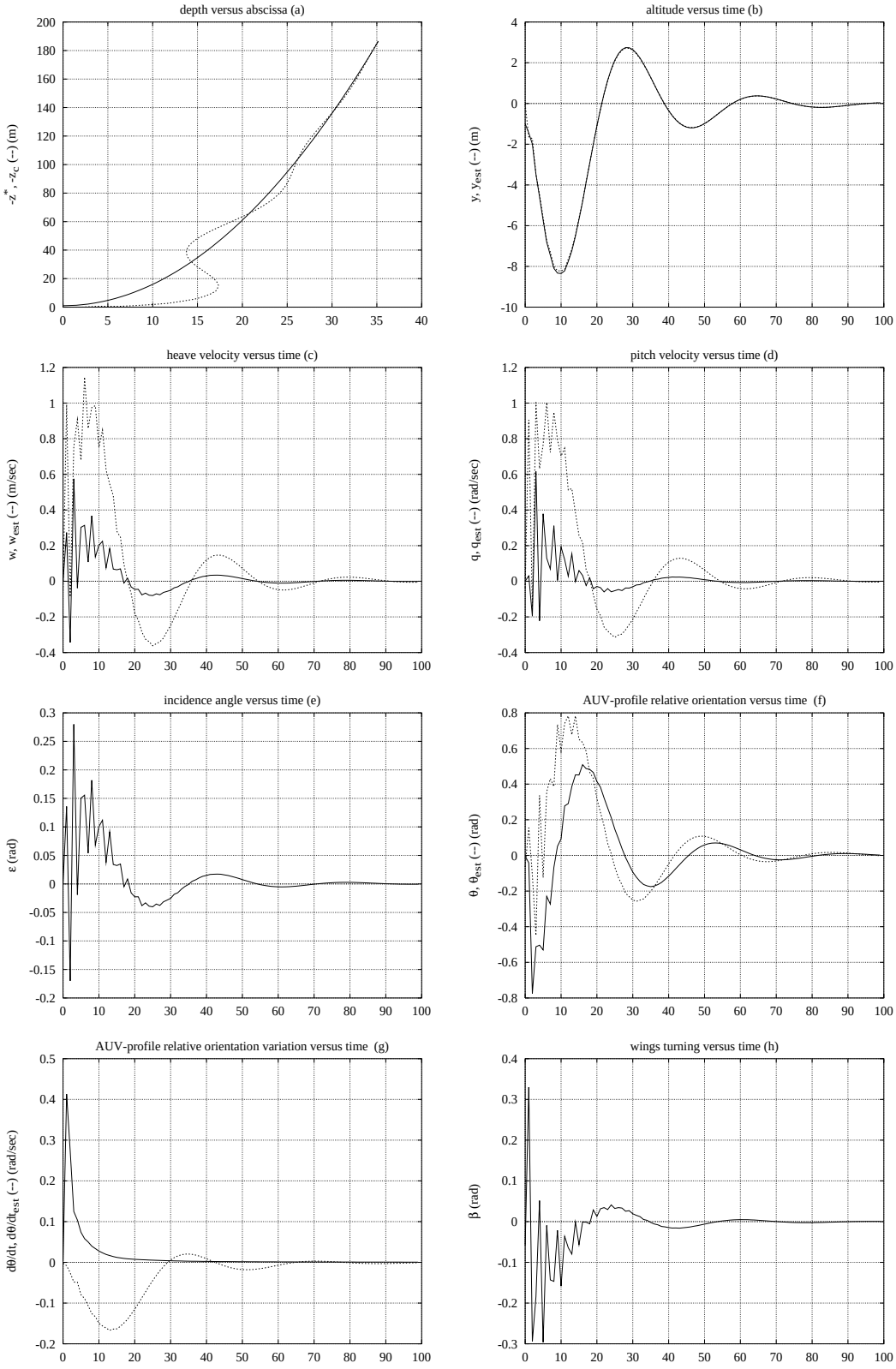

Figure 30: Simulation on parabolic bottom profile using the LQG/LTR controller. Main parameters value : bottom : $z^* = -0.15x^{*^2} + z0$, vehicle initial orientation=0rad, Rc=100.0, Ro=1.0, Ad=-.1, Cd=-Ad, Gd=5.0. Advancement velocity : $u_0 = 2m/sec$

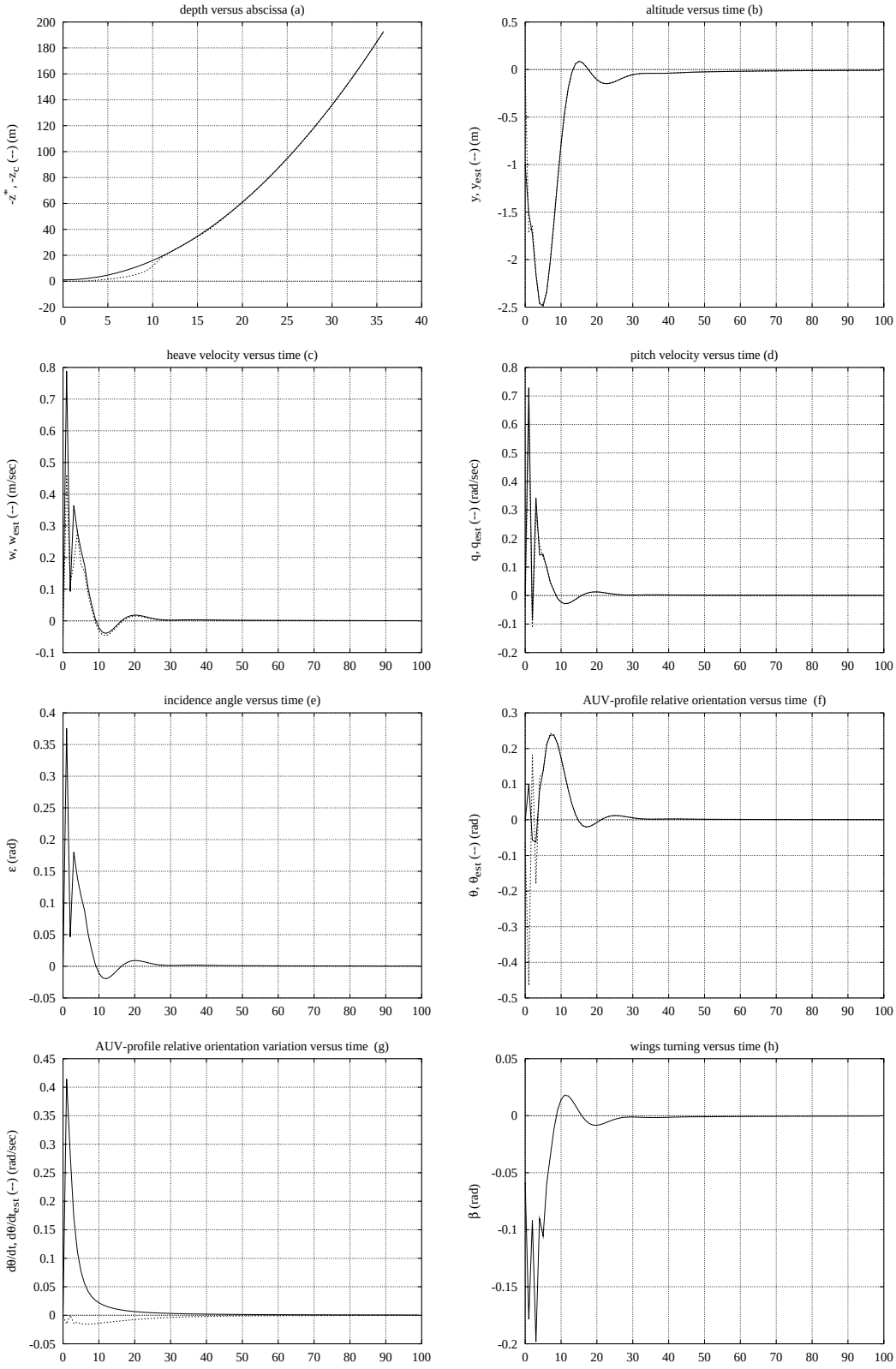

Figure 31: Simulation on parabolic bottom profile using the LQG/LTR+EKF controller. Main parameters value : bottom : $z^* = -0.15x^{*^2} + z0$, vehicle initial orientation=0rad, Rc=100.0, Ro=1.0, Ad=-.1, Cd=-Ad, Gd=5.0. Advancement velocity : $u_0 = 2m/sec$

C.5 Playing with hydrodynamic coefficients

Figures 32–33 give some results obtained when considering that the hydrodynamic coefficients C_{mw},etc , used for controller gains calculation and state estimation, are reduced by half (50%). The axial nominal advancement velocity is $u_0 = 2m/sec$, and the bottom profile is a "quasi" sinusoidal curve. Tests have been conducted with both linear LQG/LTR and LQG/LTR+EKF controllers.

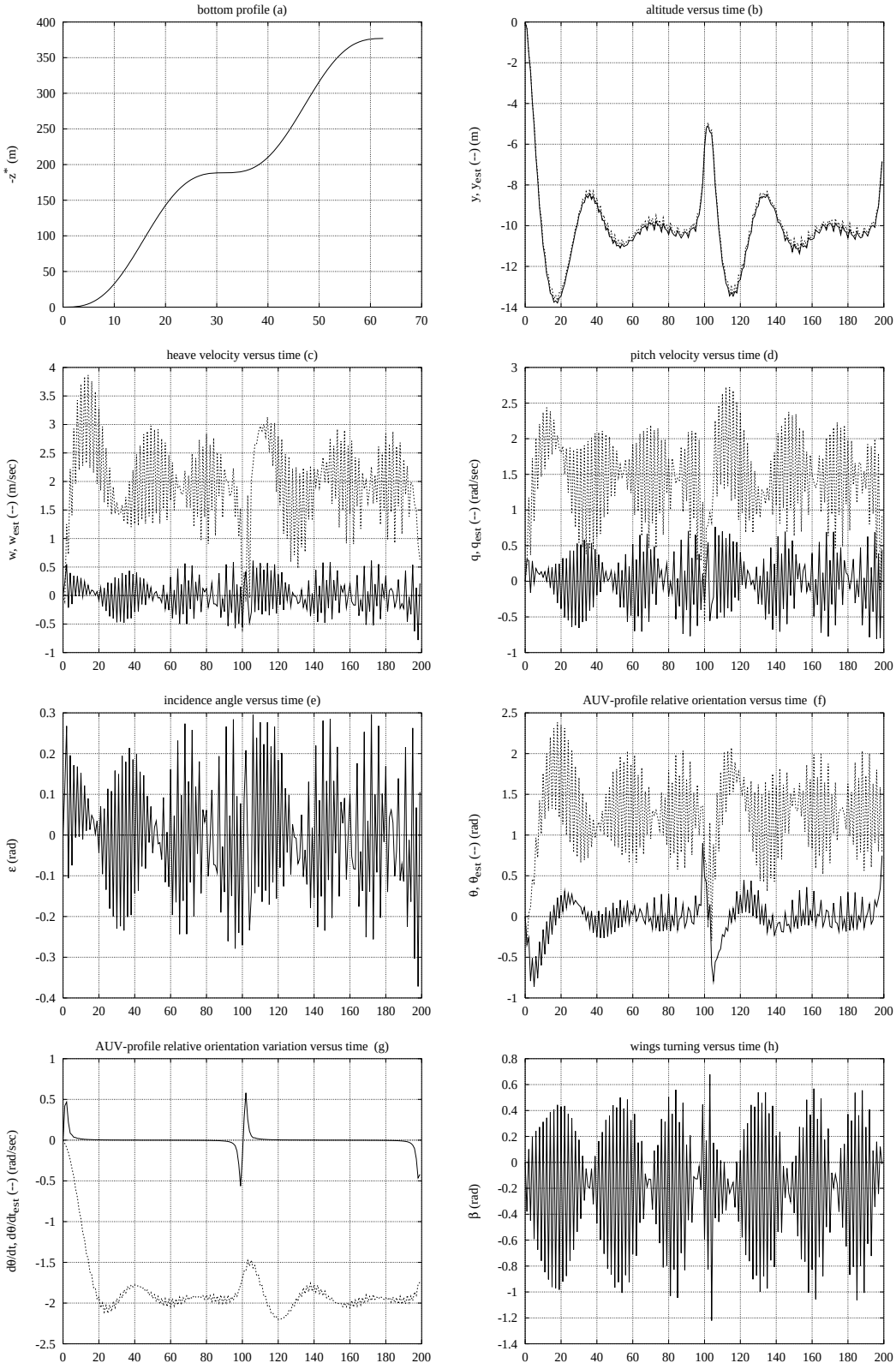

Figure 32: Simulation on "quasi" sinusoidal bottom profile using the LQG/LTR controller. Main parameters value : vehicle initial orientation=0rad, Rc=10.0, Ro=1.0, Ad=-.1, Cd=-Ad, Gd=5.0. Advancement velocity : $u_0 = 2m/sec$

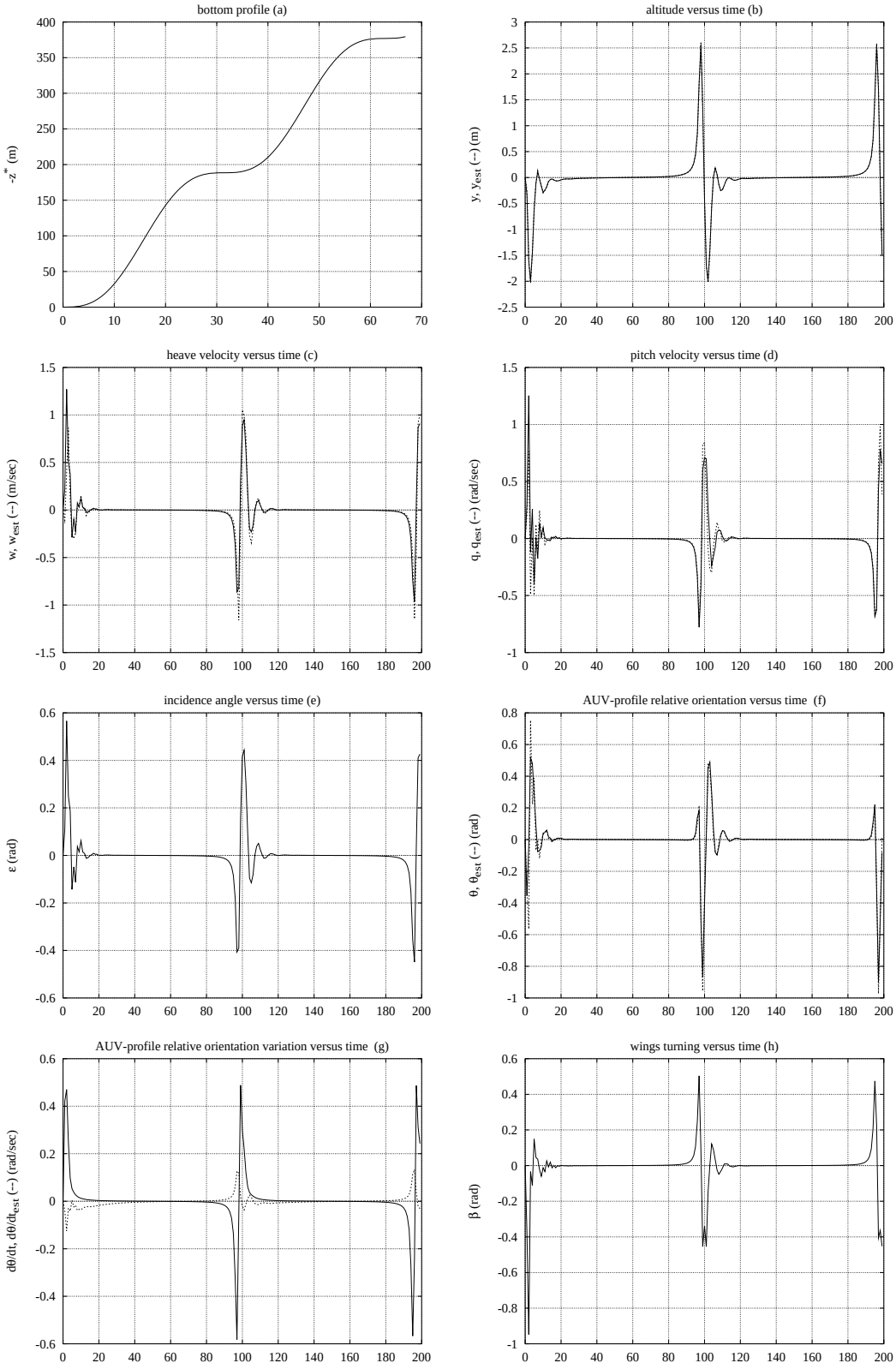

Figure 33: Simulation on "quasi" sinusoidal bottom profile using the LQG/LTR+EKF controller. Main parameters value : vehicle initial orientation=0rad, Rc=10.0, Ro=1.0, Ad=-.1, Cd=-Ad, Gd=5.0. Advancement velocity : $u_0 = 2m/sec$

References

[Anderson and Moore, 1990] Anderson, B. and Moore, J. (1990). *Optimal Control : Linear Quadratic Methods.* Prentice Hall, Englewood Cliffs NJ, USA.

[Bitmead et al., 1990] Bitmead, R., Gevers, M., and Wertz, V. (1990). *Adaptive Optimal Control : The Thinking Man's GPC.* Prentice Hall Int., Series in Systems and Control Engineering.

[Clarke and Mohtadi, 1989] Clarke, D. and Mohtadi, C. (1989). Properties of generalized predictive control. *Journal of Automatica*, 25(6):859–875.

[Clarke et al., 1987] Clarke, D., Mohtadi, C., and Tuffs, P. (1987). Generalized predictive control : Parts i and ii. *Journal of Automatica*, 23:137–160.

[Doyle et al., 1992] Doyle, J., Francis, B., and Tannenbaum, A. (1992). *Feedback control theory.* New York, Toronto, Oxford : Macmillan.

[Isidori, 1989] Isidori, A. (1989). *Nonlinear control systems.* Springer-Verlag Editions.

[Krstic et al., 1995] Krstic, M., Kanellakopoulos, I., and Kokotovic, P. (1995). *Nonlinear and adaptive control design.* John Wiley and Sons, Ltd.

[LaScala et al., 1995] LaScala, B., Bitmead, R., and James, M. (1995). Conditions for the stability of the extended kalman filter and their application to the frequency tracking problem. *Journal Mathematics of Control, Signals and Systems*, to appear.

[Masson et al., 1994] Masson, D., Sichler, B., renard, V., Michel, J., and Dias, J. (1994). An autonomous vehicle for geological exploration : sensor payload and mission analysis. In *Proc. of OCEANS'94 OSATES*, pages I–141–146.

[Mayne and Michalska, 1990] Mayne, D. and Michalska, H. (1990). Receding horizon control of nonlinear systems. *IEEE Trans. on Automatic Control*, 35(7):814–824.

[Michalska and Mayne, 1993] Michalska, H. and Mayne, D. (1993). Robust receding horizon control of constrained nonlinear systems. *IEEE Trans. on Automatic Control*, 38(11):1623–1633.

[Morari and Zafiriou, 1989] Morari, M. and Zafiriou, E. (1989). *Robust Process Control.* Prentice Hall, Englewood Cliffs NJ, USA.

[Santos et al., 1995a] Santos, A., Rives, P., Espiau, B., and Simon, D. (1995a). Dealing in real time with a priori unknown environment on autonomous underwater vehicles (auvs). In *Proc. of IEEE Int. Conf. on Robotics and Automation*, volume to appear.

[Santos et al., 1994a] Santos, A., Simon, D., and Rigaud, V. (1994a). A sensor-based high-level control approach for autonomous underwater vehicles (auvs). In *Proc. of Intelligent Robotics Systems*, pages 170–177.

[Santos et al., 1994b] Santos, A., Simon, D., and Rigaud, V. (1994b). Towards autonomous underwater vehicles (auvs) through sensor-based high level control. In *Proc. of OCEANS'94 OSATES*, volume 2, pages 113–118.

[Santos et al., 1995b] Santos, A., Simon, D., and Rigaud, V. (1995b). Sensor-based control of a class of under-actuated autonomous underwater vehicles. In *Proc. of IFAC Control Applications in Marine Systems*, volume to appear.

[Slotine and Li, 1991] Slotine, J.-J. E. and Li, W. (1991). *Applied nonlinear control*. Prentice-Hall International Editions.

Unité de recherche INRIA Lorraine, Technopôle de Nancy-Brabois, Campus scientifique,
615 rue du Jardin Botanique, BP 101, 54600 VILLERS LÈS NANCY
Unité de recherche INRIA Rennes, Irisa, Campus universitaire de Beaulieu, 35042 RENNES Cedex
Unité de recherche INRIA Rhône-Alpes, 46 avenue Félix Viallet, 38031 GRENOBLE Cedex 1
Unité de recherche INRIA Rocquencourt, Domaine de Voluceau, Rocquencourt, BP 105, 78153 LE CHESNAY Cedex
Unité de recherche INRIA Sophia-Antipolis, 2004 route des Lucioles, BP 93, 06902 SOPHIA-ANTIPOLIS Cedex

Éditeur
INRIA, Domaine de Voluceau, Rocquencourt, BP 105, 78153 LE CHESNAY Cedex (France)
ISSN 0249-6399